Supporting Information for

Phosphine-substituted diiron complexes $Fe_2(\mu\text{-Rodt})(CO)_{6-n}(PPh_3)_n$ (R = Ph, Me, H and n = 1, 2) featuring desymmetrized oxadithiolate bridges: Structures, protonation, and electrocatalysis

Xiao-Li Gu,[#] Jian-Rong Li,[#] Bo Jin, Yang Guo, Xing-Bin Jing and Pei-Hua Zhao[*]

School of Materials Science and Engineering, North University of China, Taiyuan 030051, P. R. China

*Corresponding author.

Email: zph2004@nuc.edu.cn (P.-H. Zhao).

[#]The two authors equally contributed to this work.

Contents

Part I. Crystallographic data for complexes **4** and **7-9**

Table S1. Details of crystallographic data and structure refinement for **4** and **7-9**

Complex	**4**	**7**	**8**	**9**
CCDC number	**2083414**	**2083415**	**2083416**	**2083417**
Empirical formula	$C_{31}H_{23}Fe_2O_6PS_2$	$C_{48}H_{38}Fe_2O_5P_2S_2$	$C_{43}H_{36}Fe_2O_5P_2S_2$	$C_{42}H_{34}Fe_2O_5P_2S_2$
Formula weight	698.28	932.54	870.532	856.45
Temperature (K)	150(2)	150(2)	150(2)	150(2)
Wavelength (Å)	0.71073	0.71073	0.71073	0.71073
Crystal system	triclinic	monoclinic	triclinic	triclinic
Space group	P-1	$P2_1/c$	P-1	P-1
a (Å)	9.0226(5)	14.3643(5)	9.2488(6)	9.2009(6)
b (Å)	10.2799(6)	18.3822(7)	13.4812(8)	13.4863(10)
c (Å)	17.7088(11)	17.9936(6)	17.0713(11)	16.7738(12)
α (°)	96.927(3)	90	77.746(3)	77.342(4)
β (°)	92.816(3)	110.0960(10)	89.450(3)	89.522(4)
γ (°)	115.474(2)	90	70.192(3)	70.674(4)
V (Å^3)	1462.63(15)	4461.9(3)	1952.5(2)	1911.7(2)
Z	2	4	2	2
D_{calc} (g cm^{-3})	1.586	1.388	1.481	1.488
μ (mm^{-1})	1.233	0.861	0.978	0.997
F(000)	712.0	1920.0	898.7	880.0
Crystal size (mm)	0.26×0.18×0.14	0.32×0.22×0.14	0.22×0.18×0.14	0.34 × 0.28 × 0.18
θ_{min}, θ_{max} (°)	4.444, 52.856	4.822,52.766	4.52,52.92	4.56, 52.04
Reflections collected/unique	26250/6000	76335/9129	32807/7955	42182/7545
R_{int}	0.0524	0.0415	0.0492	0.1167
hkl Range	-11 ≤ h ≤ 11	-17≤ h ≤17	-11≤ h ≤11	-11≤ h ≤11
	-12 ≤ k ≤ 12	-22 ≤ k ≤ 1622	-16 ≤ k ≤ 16	-16 ≤ k ≤ 16
	-22 ≤ l ≤ 22	-22 ≤ l ≤ 21	-21 ≤ l ≤ 21	-20 ≤ l ≤ 20
Completeness to θ_{max} (%)	99.7	99.9	98.7	100.0
Data/restraints/parameters	6000/0/379	9129/0/532	7955/0/498	7545/0/478
Goodness-of-fit (GOF) on F^2	1.013	1.074	1.035	1.141
R_1/wR_2 [$I > 2\sigma(I)$]	0.0382/0.0901	0.0742/0.2205	0.0478/0.1271	0.0717/0.1139
R_1/wR_2 (all data)	0.0608/0.1008	0.0909/0.2419	0.0744/0.1462	0.1173/0.1342
Largest difference peak/ hole (e A^{-3})	0.35/-0.31	3.53/-0.71	1.16/-0.74	0.87/-0.49

***Part II*. Additional protonation data for complexes 4-6** and **7-9**

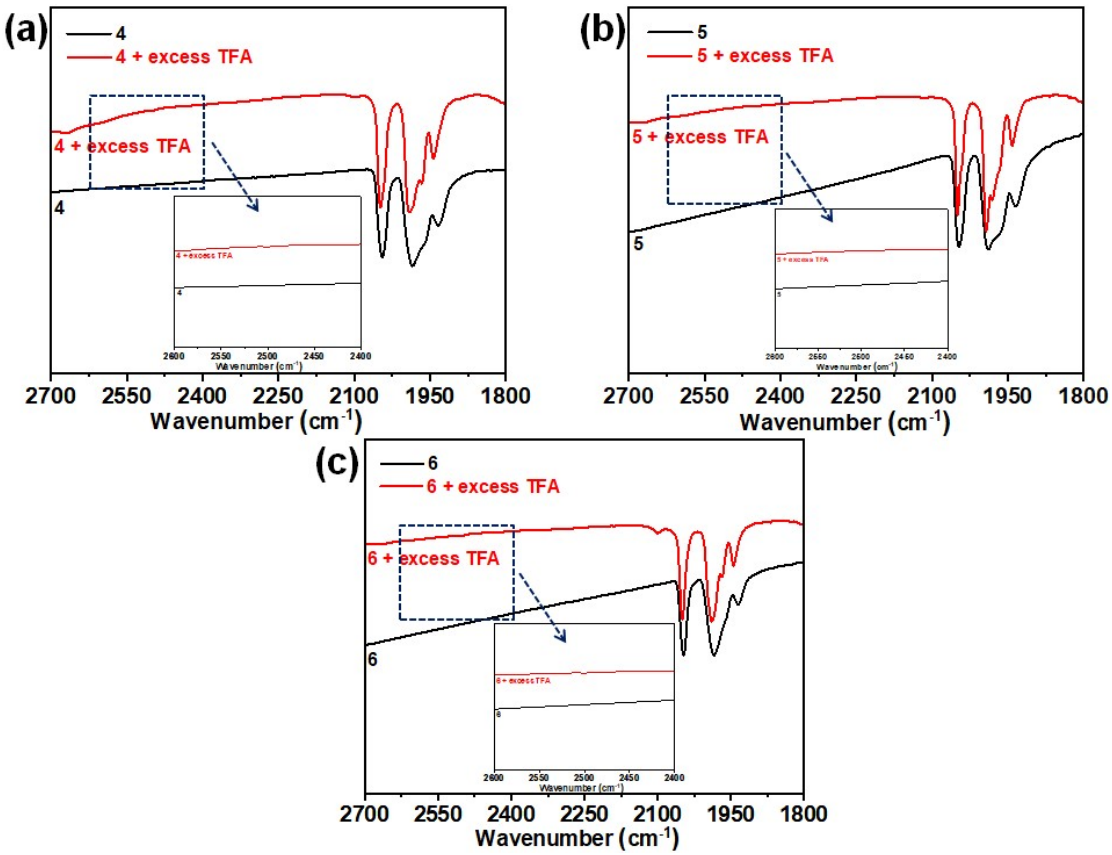

Figure S1. Comparison for FT-IR spectra (2700-1800 cm^{-1}, KBr disk) of the monosubstituted complexes **4** (a), **5** (b), and **6** (c) with 0 (black line) versus 10 (red line) equivalents of strong acid TFA. ***Insert:*** An enlarged FT-IR spectrum in the region of 2600-2400 cm^{-1} in Figures S1a-1c.

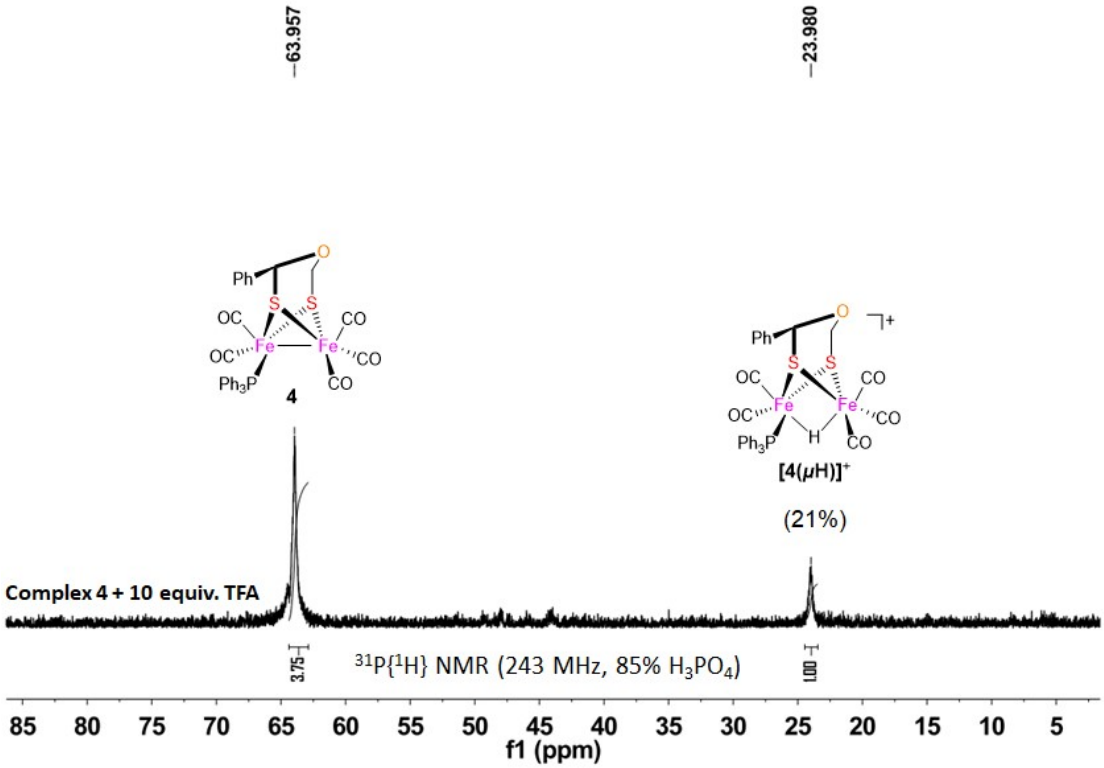

Figure S2. $^{31}P\{^{1}H\}$ NMR spectrum of the monosubstituted complex **4** (0.015 mmol) with 10 equivalents of strong acid CF_3CO_2H (TFA) in $CDCl_3$ (0.5 mL) at 298 K for 4 h. *Insert:* the proposed structure of the protonated species **[4(*μ*H)]**$^{+}$.

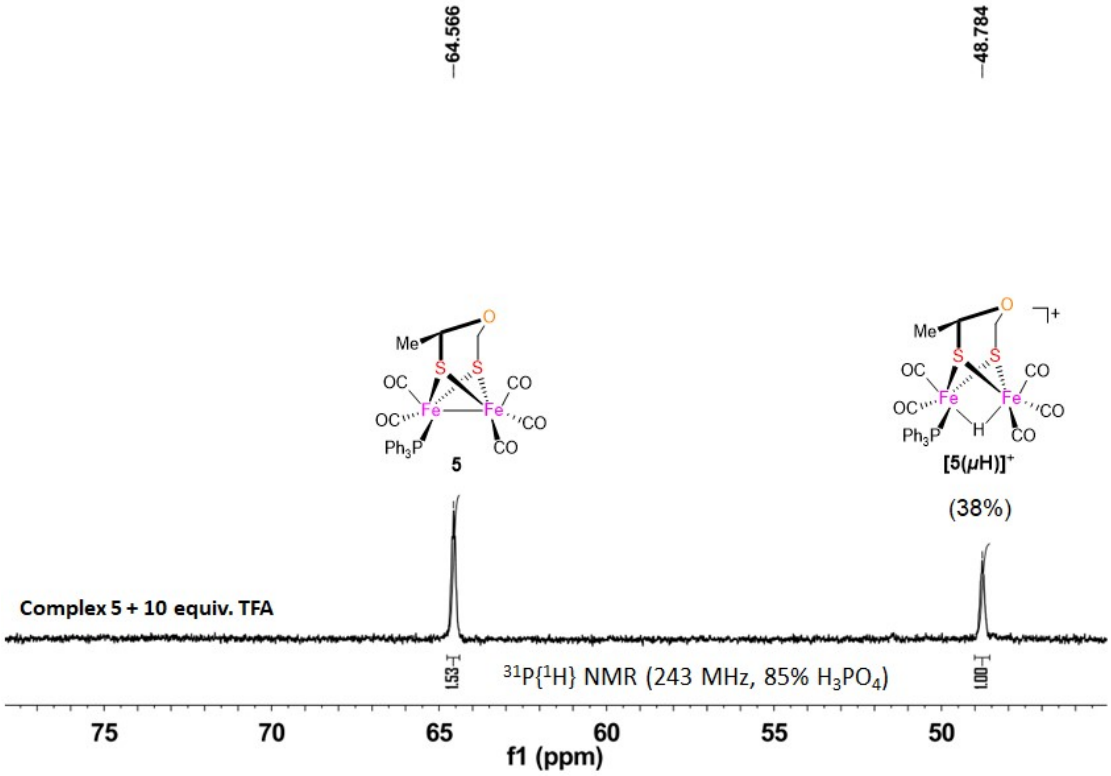

Figure S3. $^{31}P\{^{1}H\}$ NMR spectrum of the monosubstituted complex **5** (0.015 mmol) with 10 equivalents of strong acid CF_3CO_2H (TFA) in $CDCl_3$ (0.5 mL) at 298 K for 4 h. *Insert:* the proposed structure of the protonated species **[5(*μ*H)]**$^{+}$.

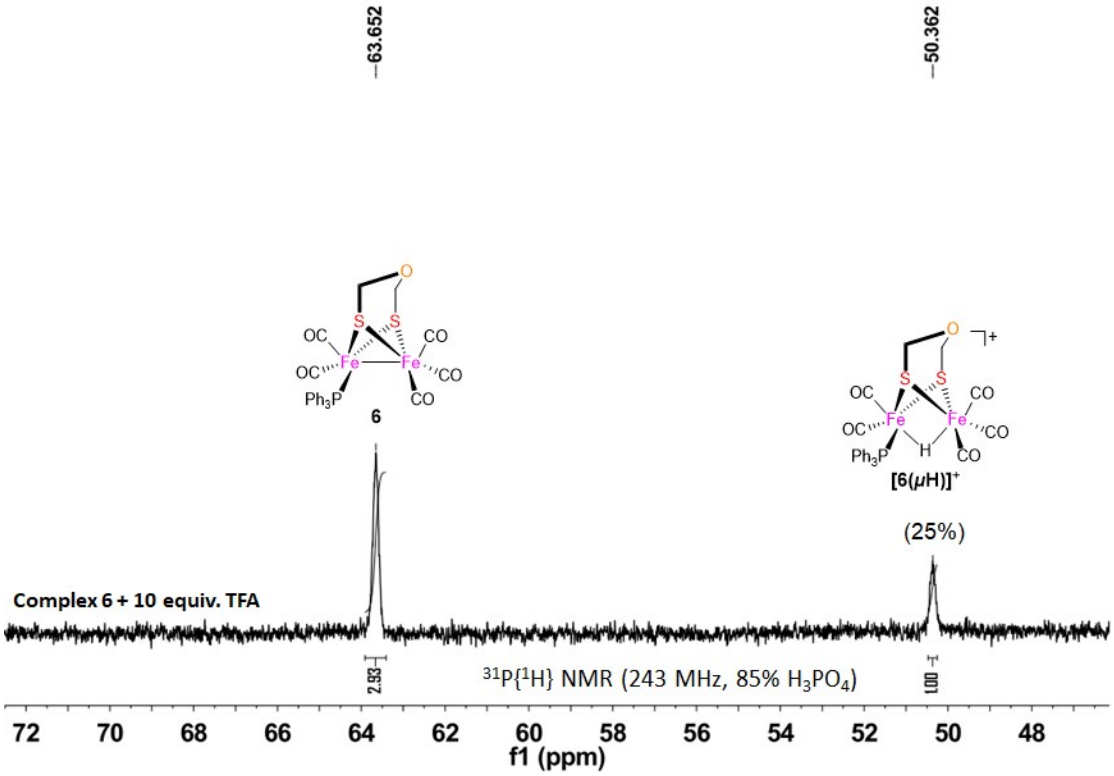

Figure S4. $^{31}P\{^{1}H\}$ NMR spectrum of the monosubstituted complex **6** (0.015 mmol) with 10 equivalents of strong acid CF_3CO_2H (TFA) in $CDCl_3$ (0.5 mL) at 298 K for 4 h. *Insert:* the proposed structure of the protonated species **[6(*μ*H)]**$^{+}$.

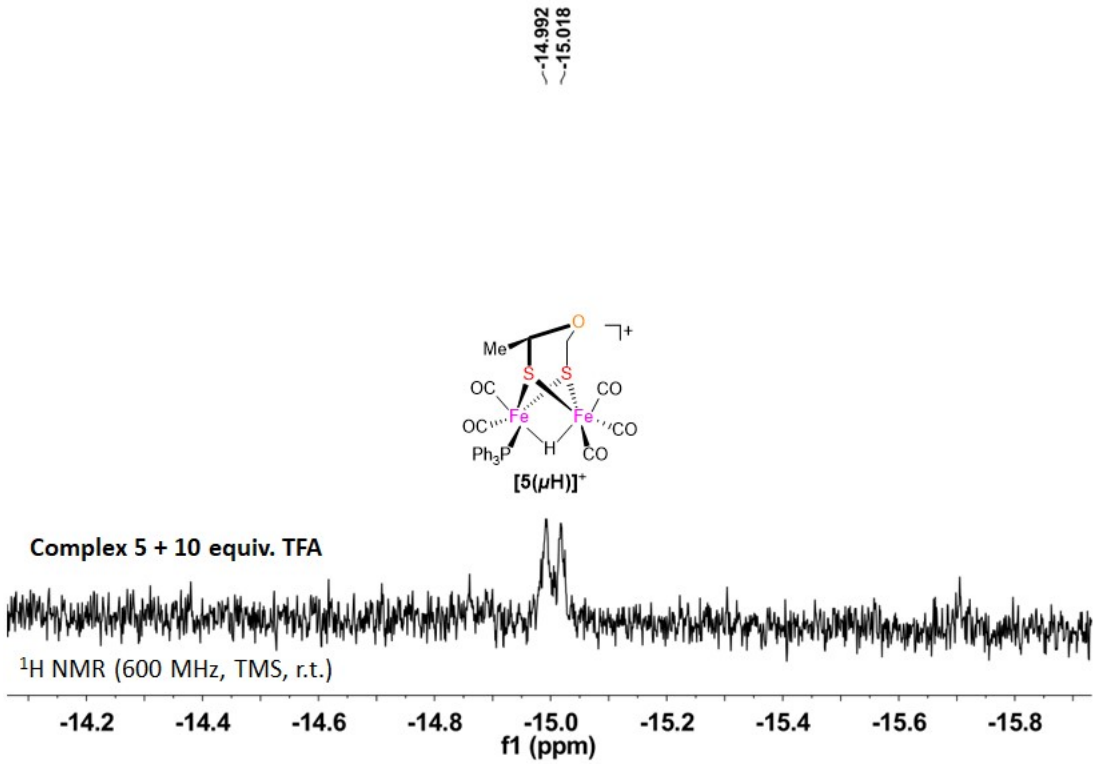

Figure S5. High-field region ^{1}H NMR spectrum of the monosubstituted complex **5** (0.015 mmol) with 10 equivalents of strong acid CF_3CO_2H (TFA) in $CDCl_3$ (0.5 mL) at 298 K for 4 h. *Insert:* the proposed structure of the protonated species **[5(*μ*H)]**$^{+}$.

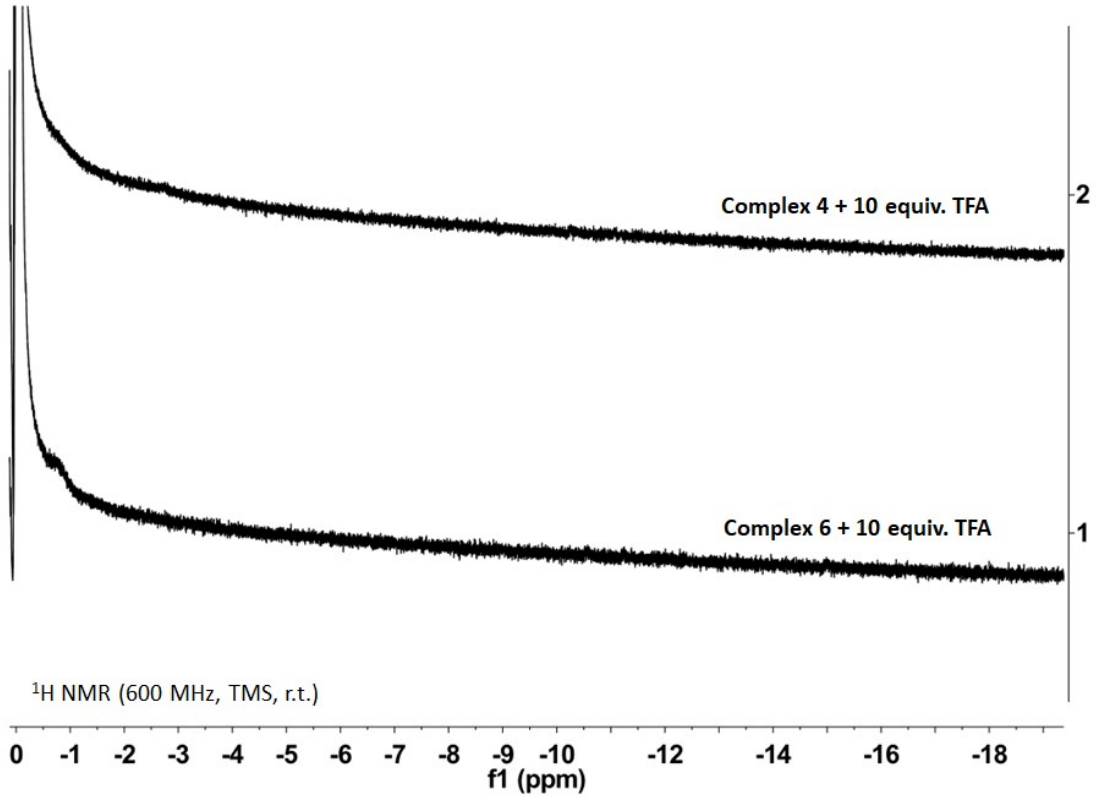

Figure S6. High-field region ^{1}H NMR spectra of the monosubstituted complexes **4** and **6** (0.015 mmol) with 10 equivalents of strong acid CF_3CO_2H (TFA) in $CDCl_3$ (0.5 mL) at 298 K for 4 h.

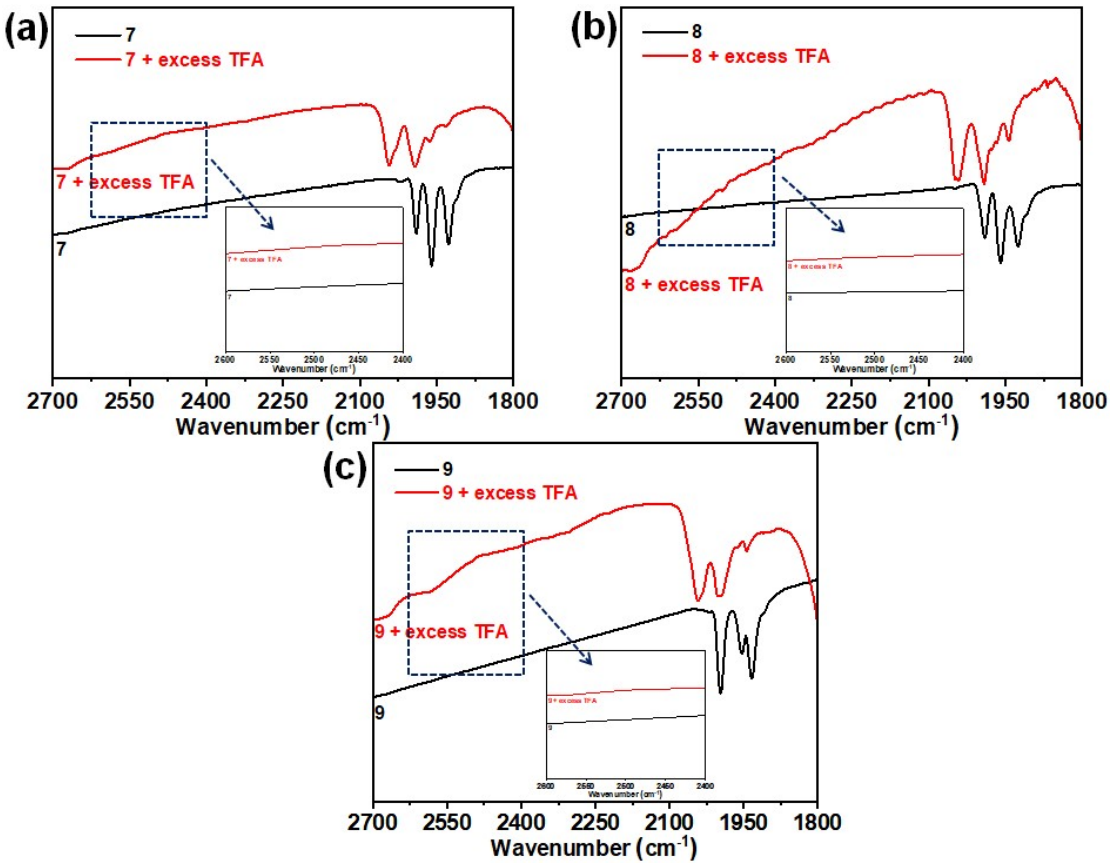

Figure S7. Comparison for FT-IR spectra (2700-1800 cm^{-1}, KBr disk) of the disubstituted complexes **7** (a), **8** (b), and **9** (c) with 0 (black line) versus 10 (red line) equivalents of strong acid TFA. ***Insert:*** An enlarged FT-IR spectrum in the region of 2600-2400 cm^{-1} in Figures S7a-7c.

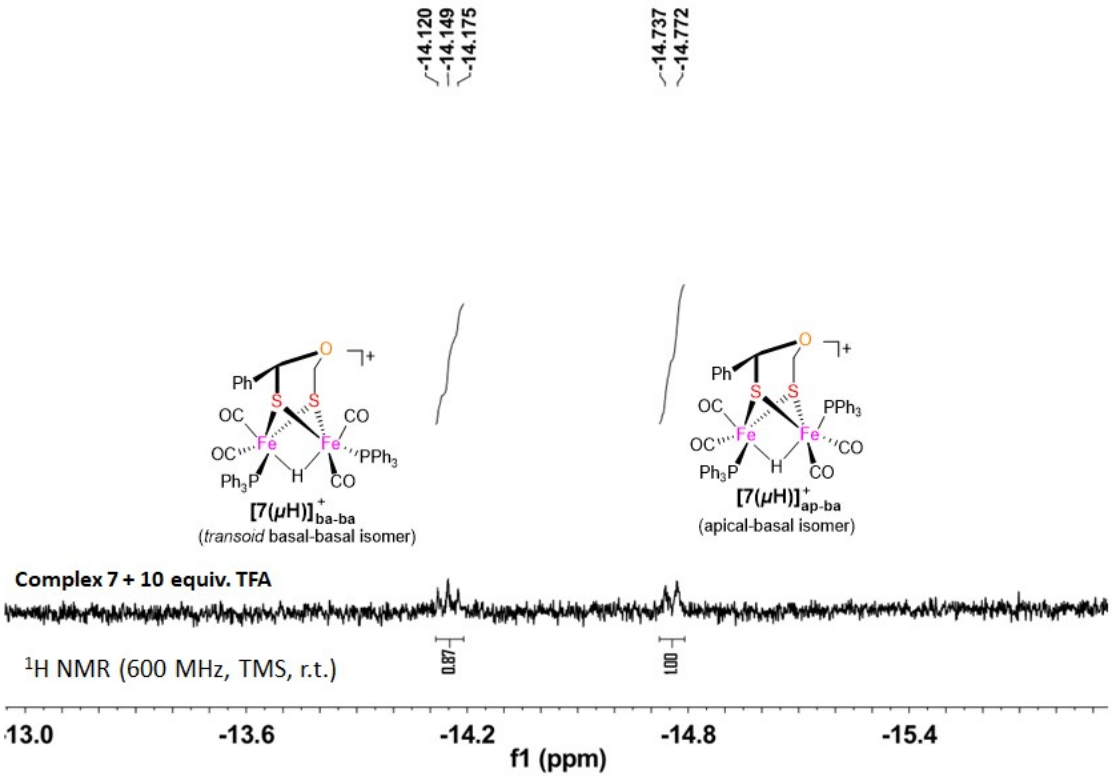

Figure S8. High-field region ^{1}H NMR spectrum of the disubstituted complex **7** (0.015 mmol) with 10 equivalents of strong acid CF_3CO_2H (TFA) in $CDCl_3$ (0.5 mL) at 298 K for 3 h. *Insert*: The proposed isomeric structures of the protonated species **[7(*μ*H)]**$^{+}$.

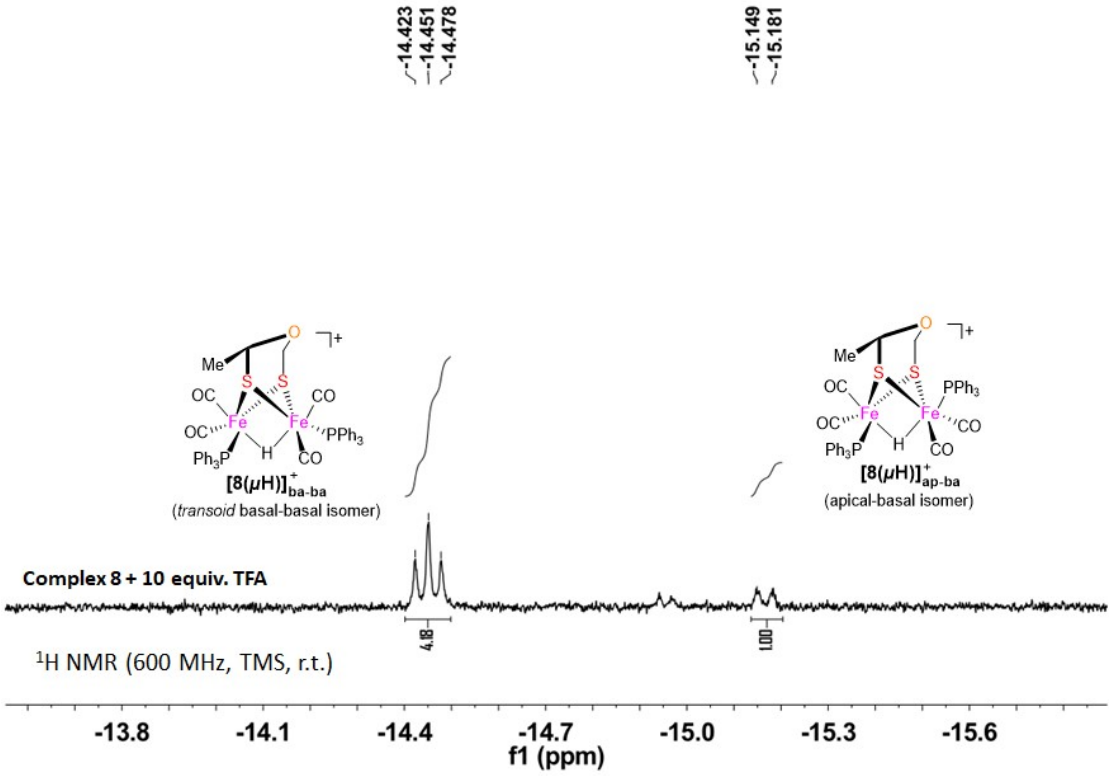

Figure S9. High-field region ^{1}H NMR spectrum of the disubstituted complex **8** (0.015 mmol) with 10 equivalents of strong acid CF_3CO_2H (TFA) in $CDCl_3$ (0.5 mL) at 298 K for 3 h. *Insert*: The proposed isomeric structures of the protonated species **[8(*μ*H)]**$^{+}$.

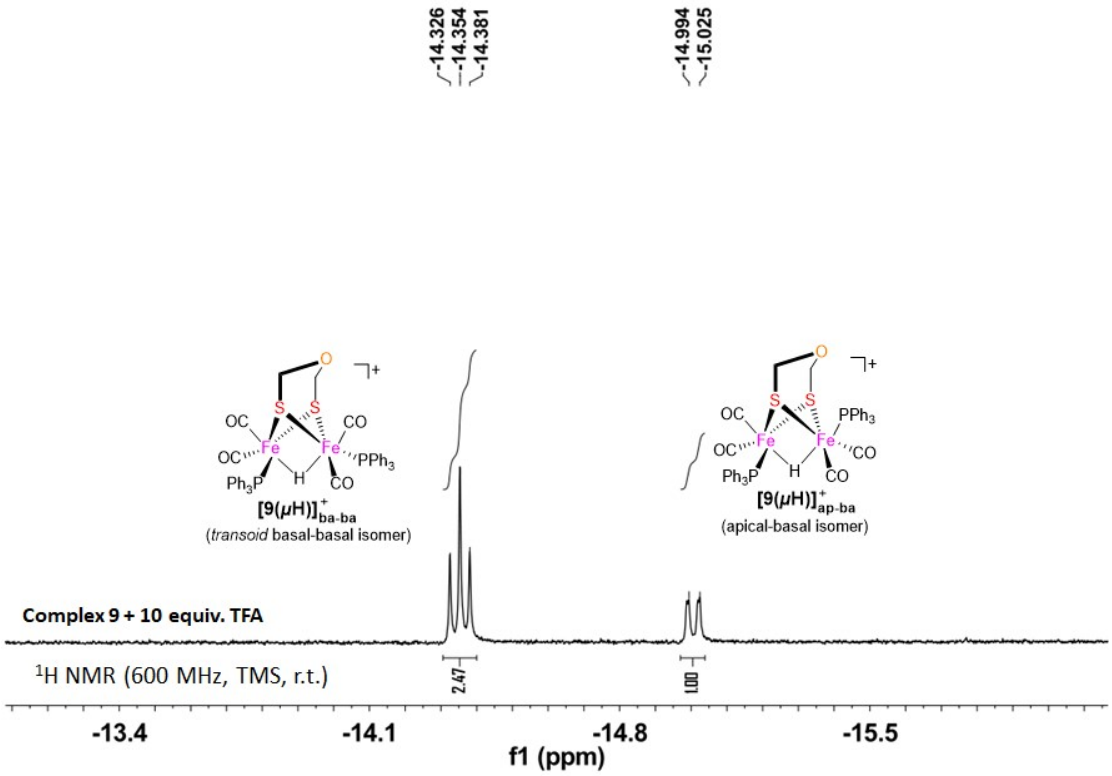

Figure S10. High-field region ^{1}H NMR spectrum of the disubstituted complex **9** (0.015 mmol) with 10 equivalents of strong acid CF_3CO_2H (TFA) in $CDCl_3$ (0.5 mL) at 298 K for 3 h. *Insert*: The proposed isomeric structures of the protonated species **[9(*μ*H)]**$^{+}$.

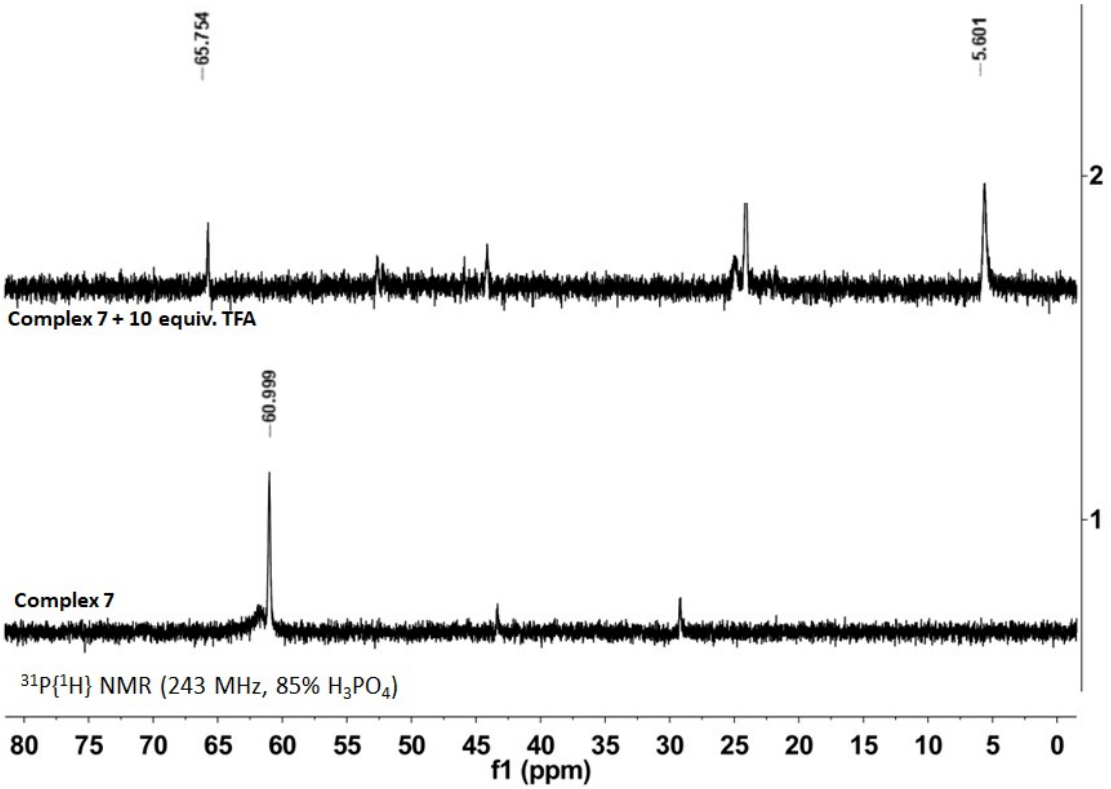

Figure S11. $^{31}P\{^{1}H\}$ NMR spectra of the disubstituted complex **7** (0.015 mmol) with 0 versus 10 equivalents of strong acid CF_3CO_2H (TFA) in $CDCl_3$ (0.5 mL) at 298 K for 3 h. *Insert*: The proposed isomeric structures of the protonated species **[7(*μ*H)]**$^{+}$.

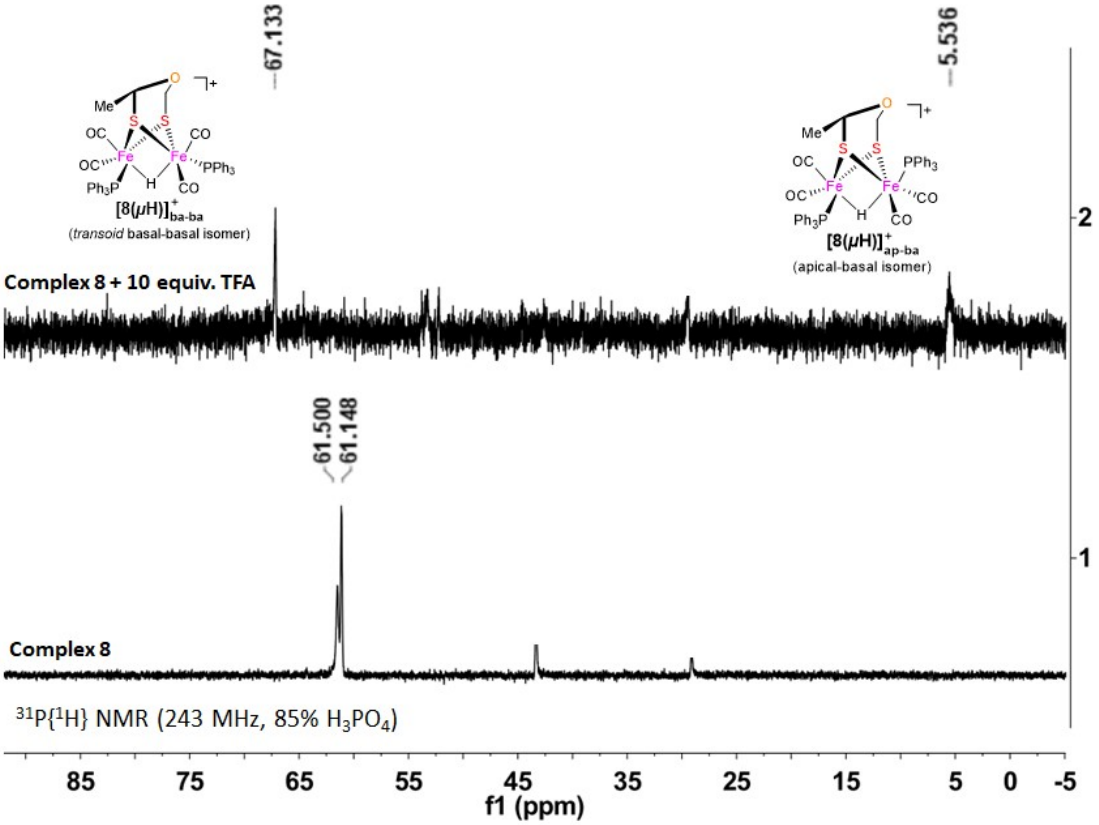

Figure S12. $^{31}P\{^{1}H\}$ NMR spectra of the disubstituted complex **8** (0.015 mmol) with 0 versus 10 equivalents of strong acid CF_3CO_2H (TFA) in $CDCl_3$ (0.5 mL) at 298 K for 3 h. *Insert*: The proposed isomeric structures of the protonated species **[8(*μ*H)]**$^{+}$.

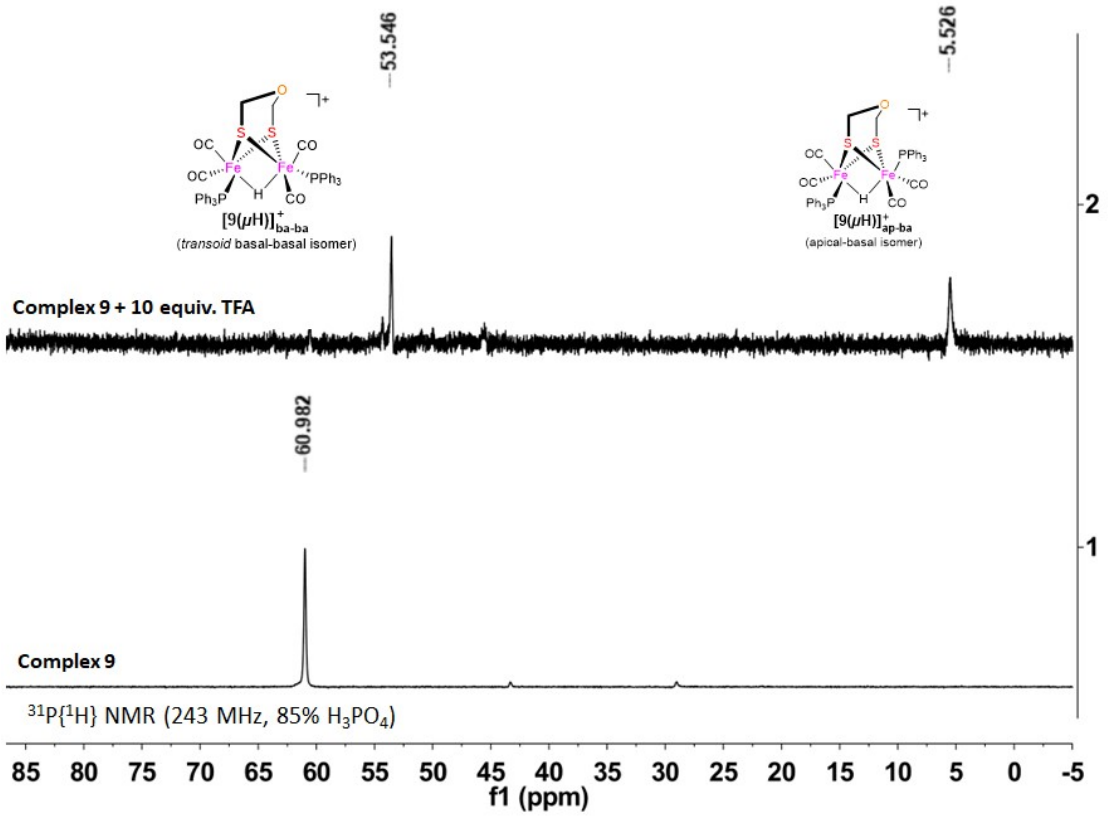

Figure S13. $^{31}P\{^{1}H\}$ NMR spectra of the disubstituted complex **9** (0.015 mmol) with 0 versus 10 equivalents of strong acid CF_3CO_2H (TFA) in $CDCl_3$ (0.5 mL) at 298 K for 3 h. *Insert*: The proposed isomeric structures of the protonated species **[9(*μ*H)]**$^{+}$.

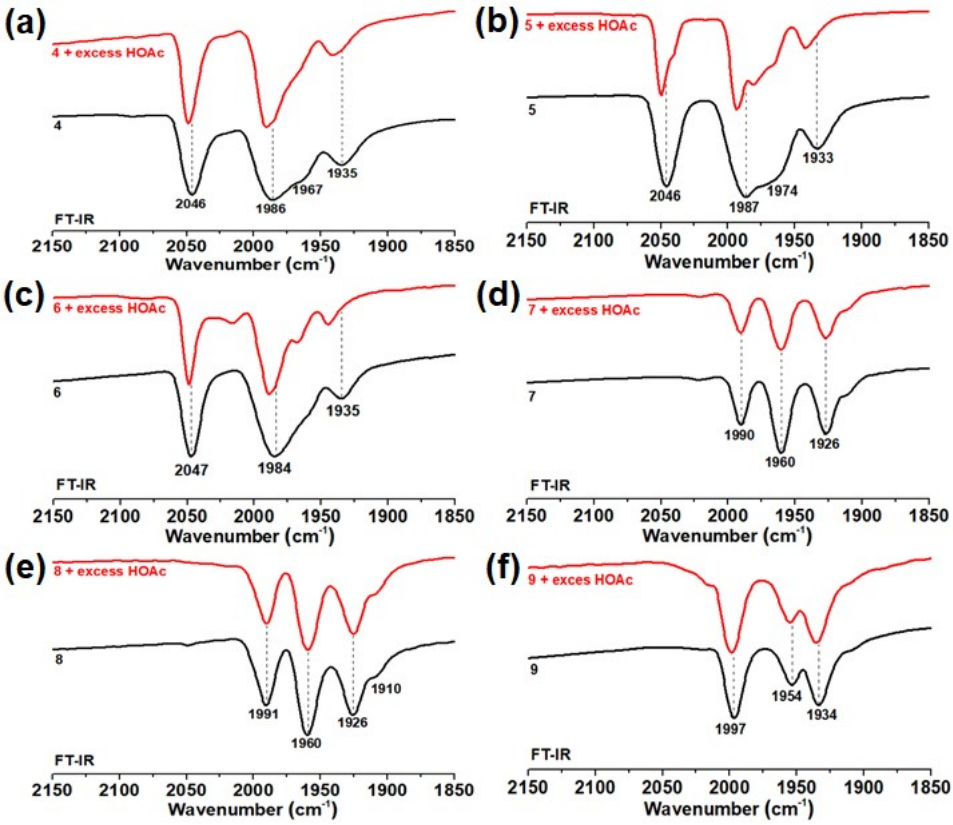

Figure S14. FT-IR spectra (a-f) recorded for the *in situ* protonations of the mono- and disubstituted complexes **4**-**6** and **7**-**9** (0.015 mmol) with 0 (black line) versus 10 (red line) equivalents of weak acid CH_3CO_2H (HOAc) in 5 mL CH_2Cl_2 at 298 K for 8 h, respectively.

Part III. Electrolysis experiments and TONs calculations of complexes 4-6 and 7-9

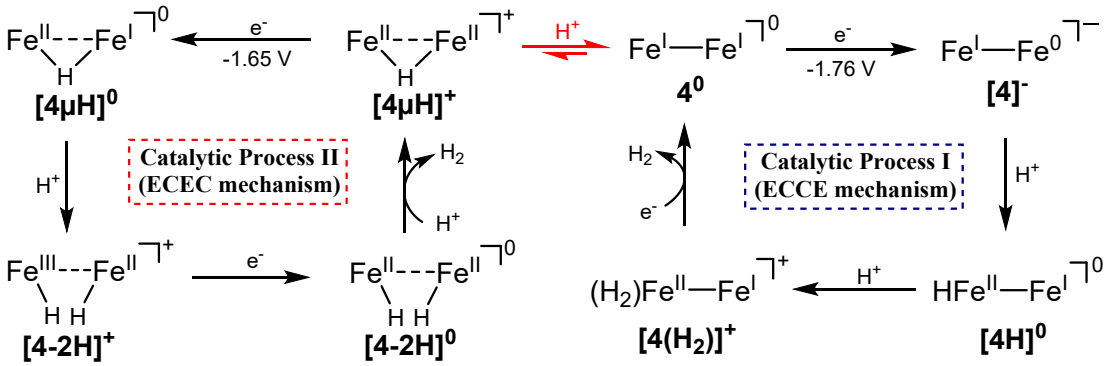

Scheme S1. Two electrocatalytic proton reduction processes I and II of a representative precursor **4** (for the monosubstituted complexes **4**-**6**) at E_{pc1} = -1.76 V through a proposed ECCE mechanism and at E_{pc3} = -1.65 V through a suggested ECEC mechanism in the presence of TFA as a proton source, respectively, wherein the Rodt, CO, and PPh_3 ligands are omitted for clarity.

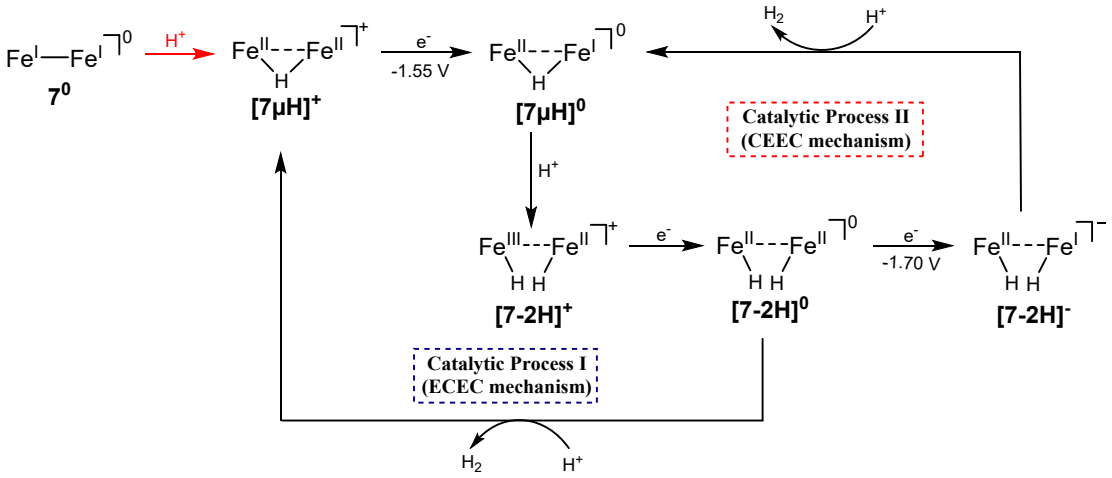

Scheme S2. Two electrocatalytic proton reduction processes I and II of a representative precursor **7** (for the disubstituted complexes **7**-**9**) at E_{pc3} = -1.55 V through a proposed ECEC mechanism and at E_{pc4} = -1.70 V through a suggested CEEC mechanism in the presence of TFA as a proton source, respectively, wherein the Rodt, CO, and PPh_3 ligands are omitted for clarity.

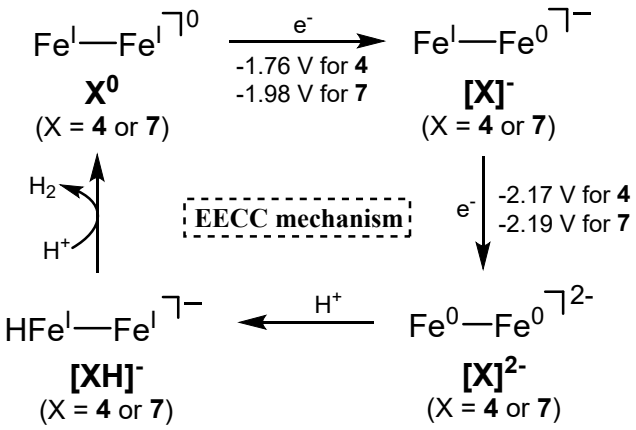

Scheme S3. Electrocatalytic proton reduction process of two representative precursors **4** (for the monosubstituted complexes **4**-**6**) at E_{pc2} = -2.17 V and **7** (for the disubstituted complexes **7**-**9**) at E_{pc2} = -2.19 V via a suggested EECC mechanism in the presence of HOAc as a proton source, respectively, wherein the Rodt, CO, and PPh_3 ligands are omitted for clarity.

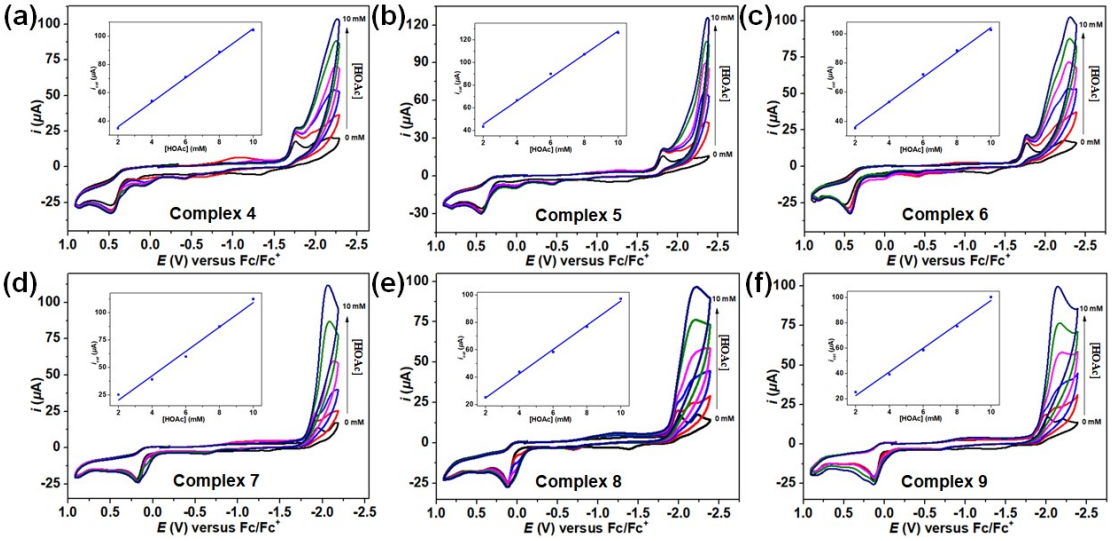

Figure S15. CV curves of 1.0 mM complexes **4-6** (a-c) and **7-9** (e-f) with weak acid HOAc (0–10 mM) in 0.1 M *n*-Bu_4NPF_6/MeCN at a scan rate of 0.05 V s^{-1}. *Inserts* in (a-c) and (e-f): Plots of catalytic currents (i_{cat}, μA) of **4-6** and **7-9** with increasing acid concentrations ([HOAc], mM), respectively. All potentials are versus the ferrocene/ferrocenium ($Fc^{0/+}$) couple.

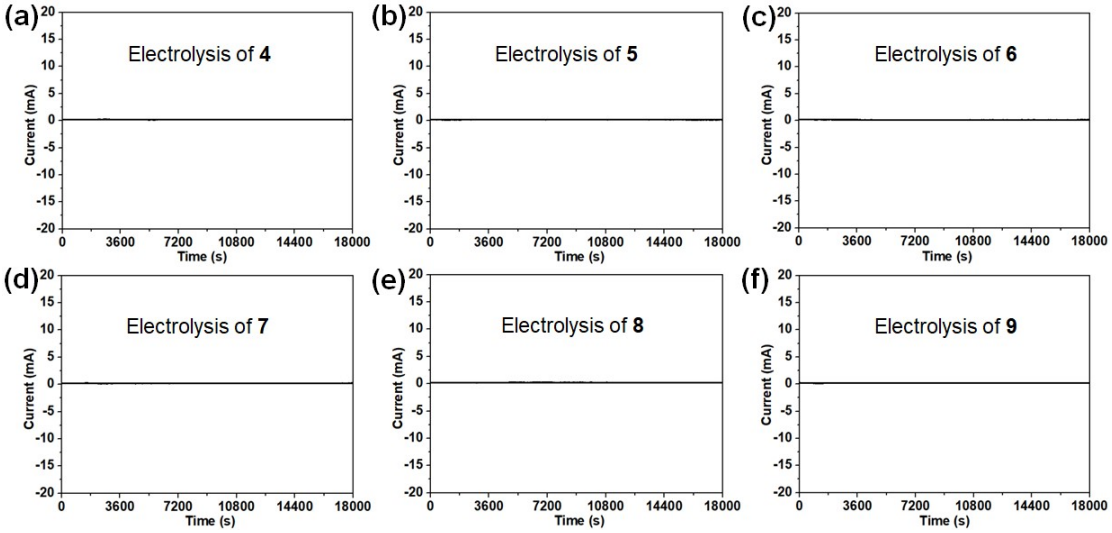

Figure S16. Controlled-potential electrolysis experiments (i-t curves) of complexes **4**-**6** (0.5 mM, a-c) and **7**-**9** (0.5 mM, d-f) in 5 mM strong acid TFA/MeCN solution for 5 h at -2.30 V vs. $Ag/AgNO_3$.

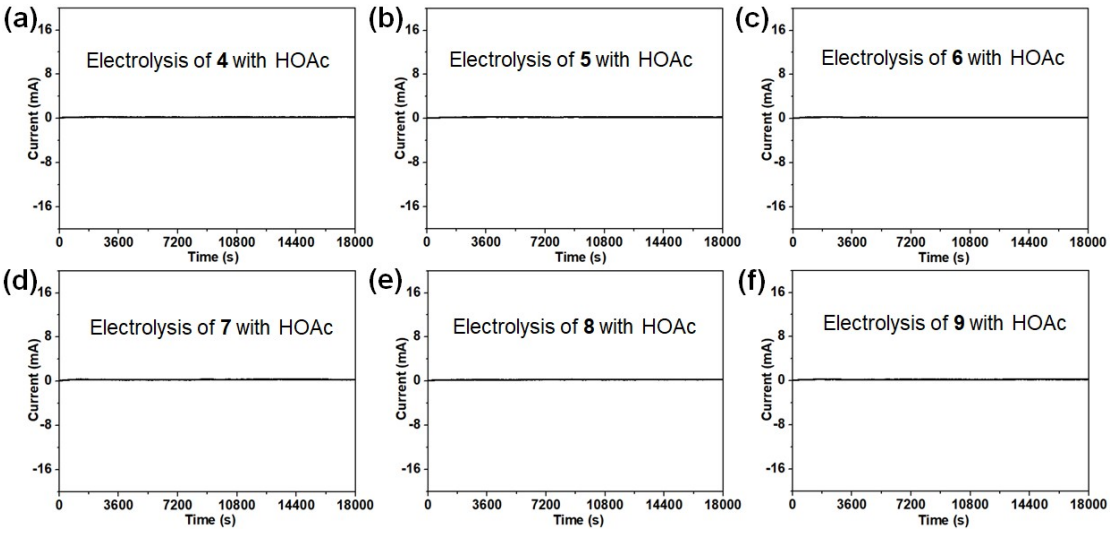

Figure S17. Controlled-potential electrolysis experiments (i-t curves) of complexes **4**-**6** (0.5 mM, a-c) and **7**-**9** (0.5 mM, d-f) in 5 mM weak acid HOAc/MeCN solution for 5 h at -2.30 V vs. $Ag/AgNO_3$.

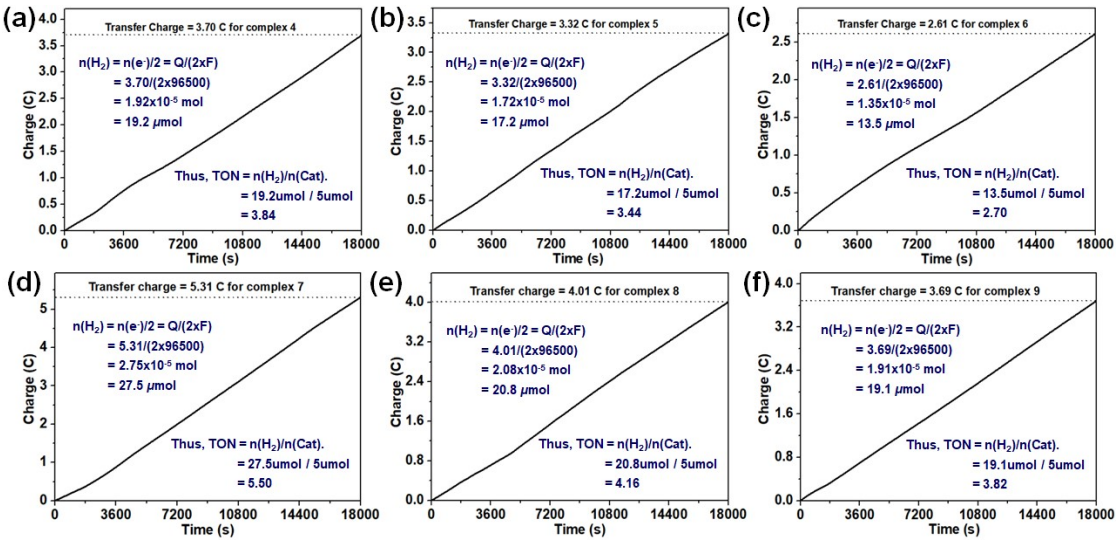

Figure S18. Q-t curves and TONs calculations of complexes **4-6** (0.5 mM, a-c) and **7-9** (0.5 mM, d-f) in 5 mM strong acid TFA/MeCN solution for 5 h at -2.30 V vs. $Ag/AgNO_3$, respectively.

TON calculation for complex 4 as a representive example [1,2]:

(1) From the CPE experiment shown in Fig. S15a, the total charges passed for complex **4** are equal to 3.70 C with 5 hours. Thus, we converted this charge into the moles of transfer electron on the GCE electrode (division by faraday constant F), *i.e.*, $n(e^-) = Q/F$ ($F = 96500\ C \cdot mol^{-1}$). According to the reaction $2H^+ + 2e^- = H_2$, the moles of H_2 produced is estimated from the moles of transfer electron on the GCE electrode (division by 2), *i.e.*, $n(H_2) = n(e^-)/2 = Q/(2xF)$. Thus, $n(H_2) = 3.70 / (2x96500) = 1.92x10^{-5}$ mol = 19.2 μmol for complex 4.

(2) According to the equations: $TON = n(H_2)/n(catalyst)$, TON = 19.2 μmol / 5 μmol = 3.84 for complex 4

References:

[1] A. Le Goff, V. Artero, B. Jousselme, P. D. Tran, N. Guillet, R. Métayé, A. Fihri, S. Palacin and M. Fontecave, From hydrogenases to noble metal–free catalytic nanomaterials for H_2 production and uptake, *Science*, 2009, **326**, 1384−1387.

[2] S. Dey, A. Rana, S. G. Dey and A. Dey, Electrochemical hydrogen Production in acidic water by an azadithiolate bridged synthetic hydrogenese mimic: Role of aqueous solvation in lowering overpotential, *ACS Catal.*, 2013, **3**, 429−436.

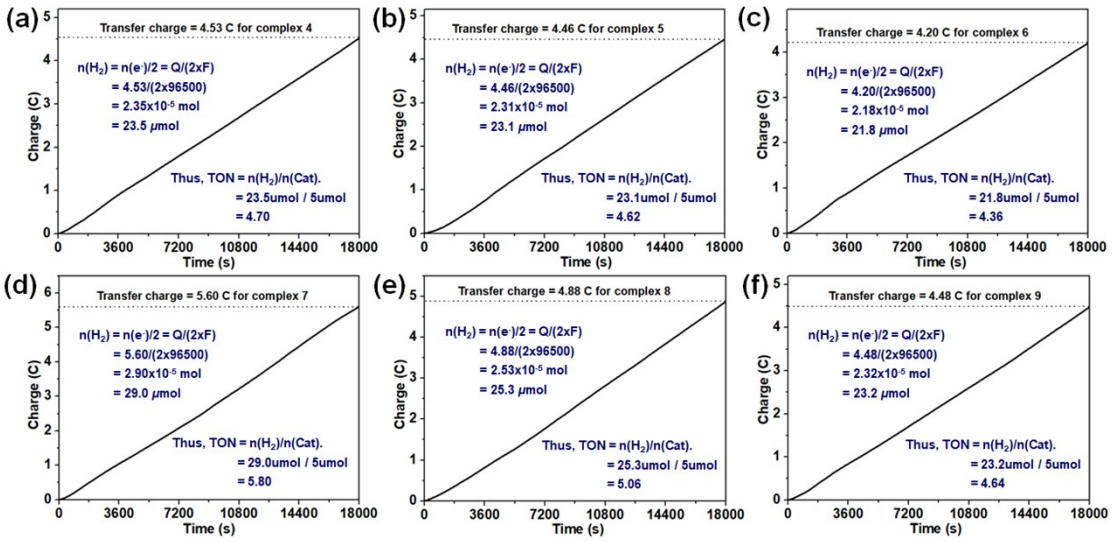

Figure S19. Q-t curves and TONs calculations of complexes **4**-**6** (0.5 mM, a-c) and **7**-**9** (0.5 mM, d-f) in 5 mM weak acid HOAc/MeCN solution for 5 h at -2.30 V vs. $Ag/AgNO_3$, respectively.

***Part IV*. The IR and NMR spectra for complexes 1, 2, 4-6 and 7-9**

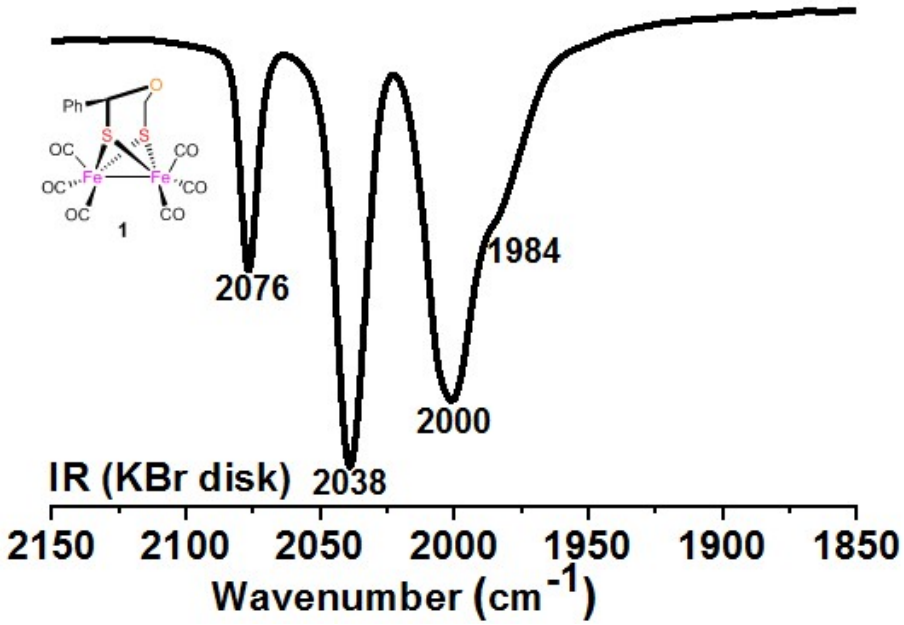

Figure S20. FT-IR spectrum of $Fe_2(\mu$-Phodt)$(CO)_6$ (**1**) in KBr.

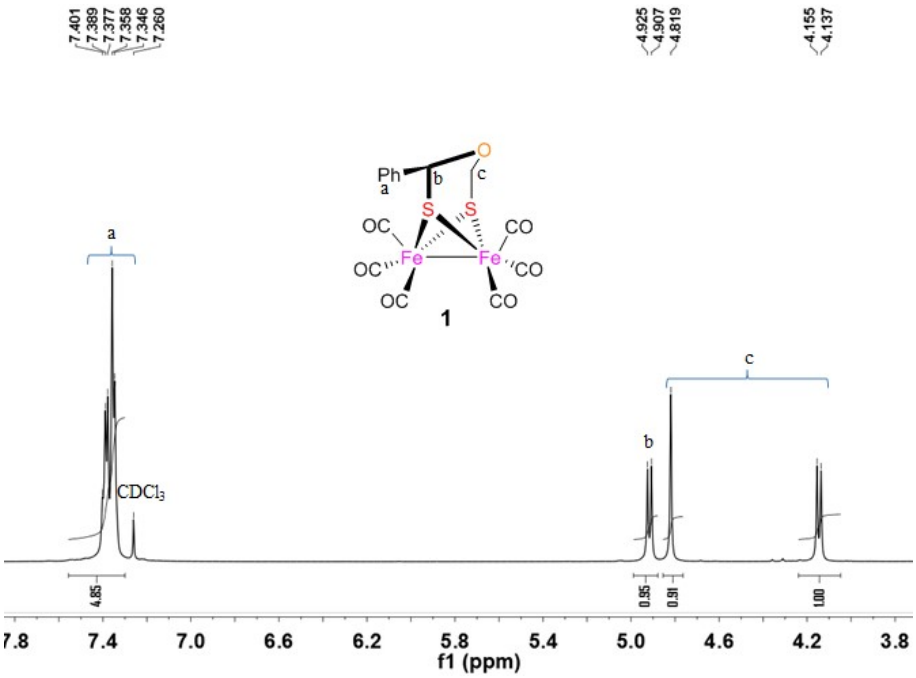

Figure S21. ^{1}H NMR spectrum of $Fe_2(\mu$-Phodt$)(CO)_6$ (**1**) in $CDCl_3$ (600 MHz, TMS).

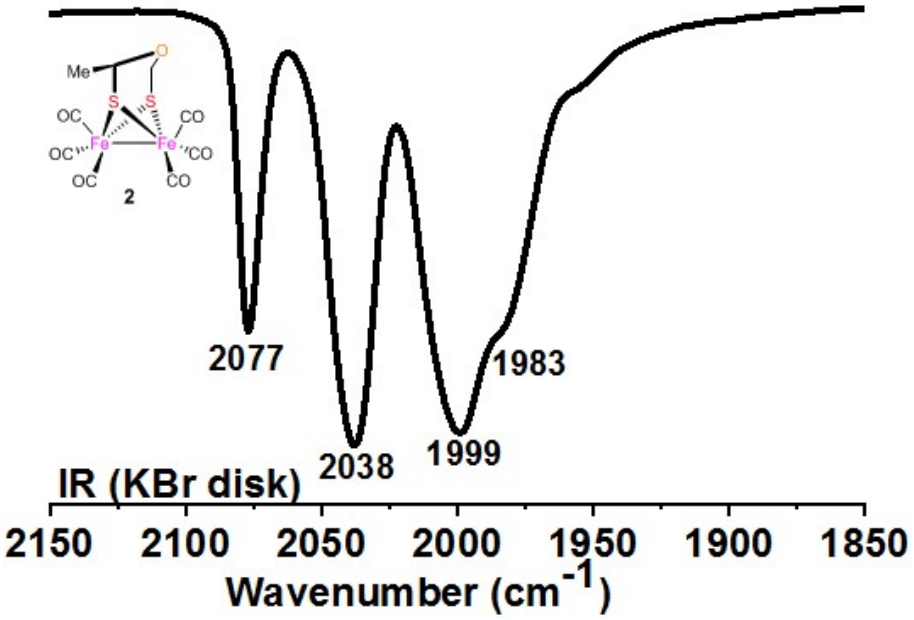

Figure S22. FT-IR spectrum of $Fe_2(\mu$-Meodt$)(CO)_6$ (**2**) in KBr.

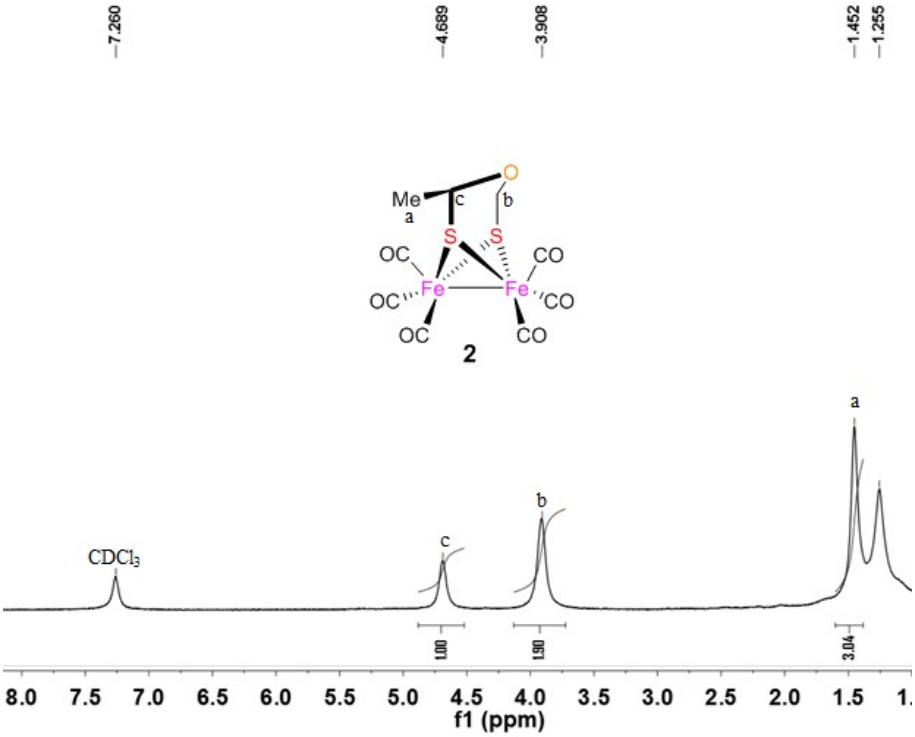

Figure S23. ^{1}H NMR spectrum of $Fe_2(\mu$-Meodt)$(CO)_6$ (**2**) in $CDCl_3$ (600 MHz, TMS).

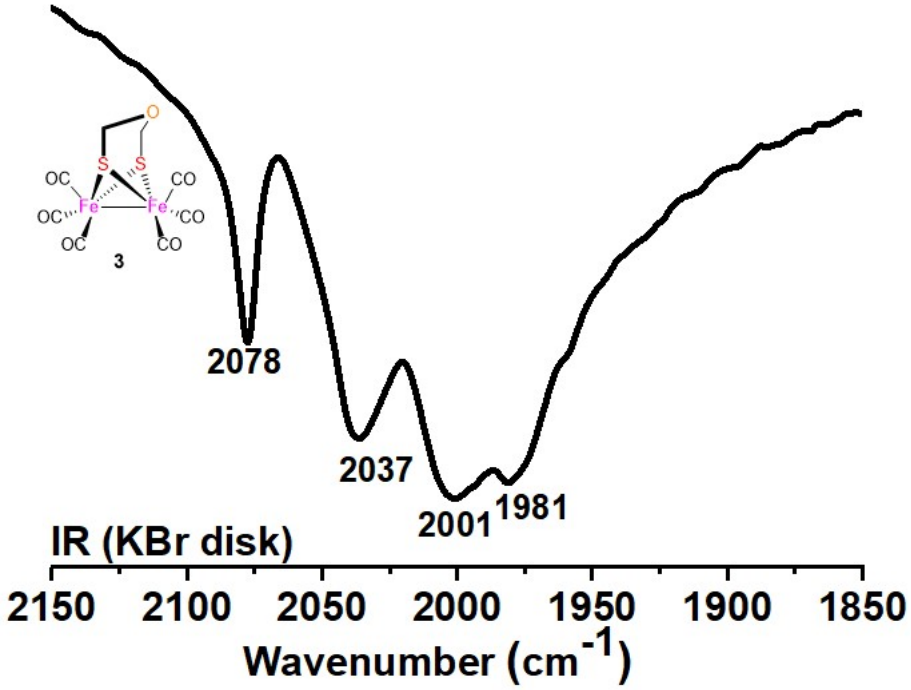

Figure S24. FT-IR spectrum of $Fe_2(\mu\text{-odt})(CO)_6$ (**3**) in KBr.

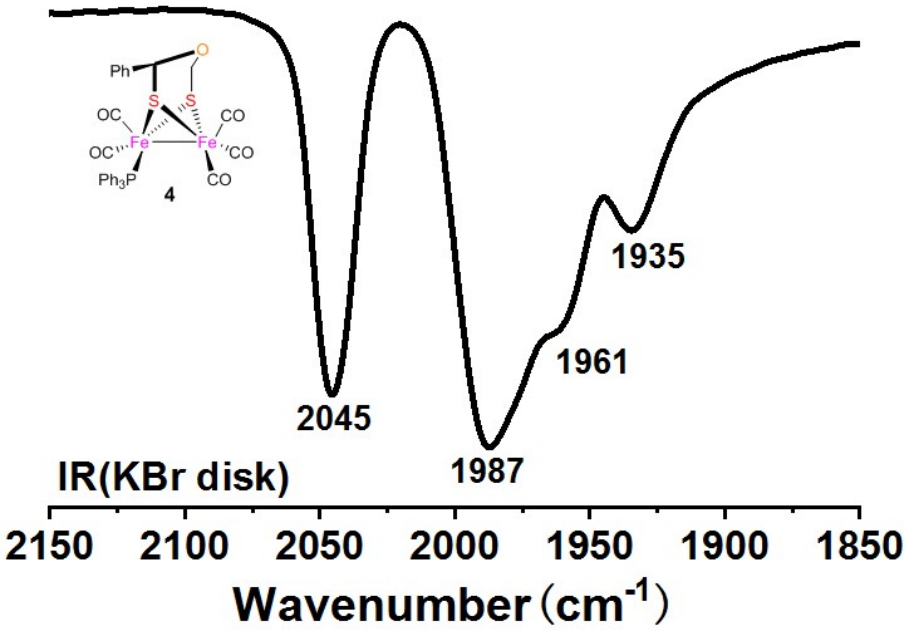

Figure S25. FT-IR spectrum of $Fe_2(\mu$-Phodt)$(CO)_5(PPh_3)$ (**4**) in KBr.

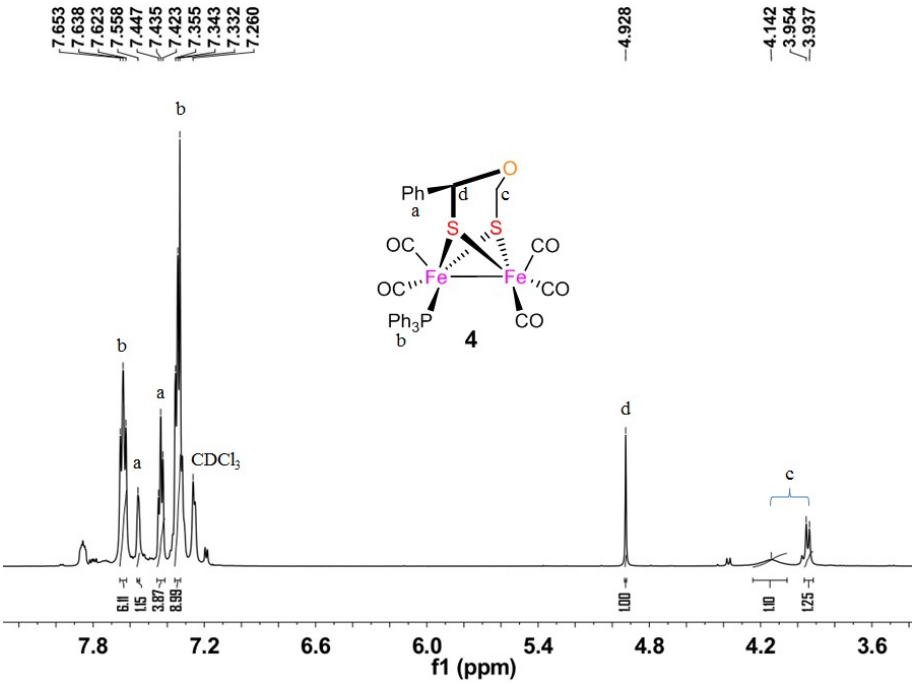

Figure S26. ^{1}H NMR spectrum of $Fe_2(\mu\text{-Phodt})(CO)_5(PPh_3)$ (**4**) in $CDCl_3$ (600 MHz, TMS).

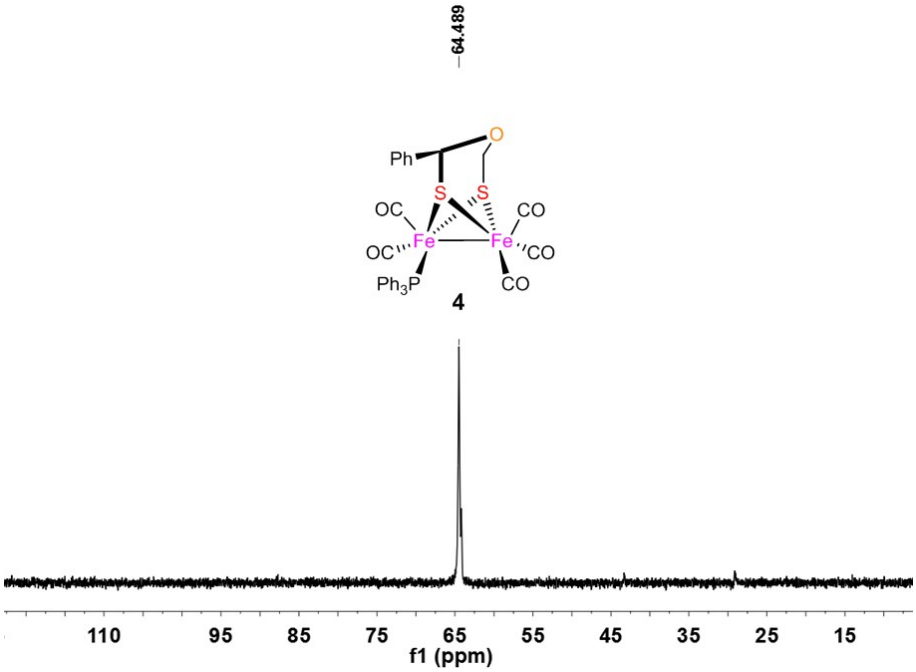

Figure S27. $^{31}P\{^{1}H\}$ NMR spectrum of $Fe_2(\mu\text{-Phodt})(CO)_5(PPh_3)$ (**4**) in $CDCl_3$ (243 MHz, 85% H_3PO_4).

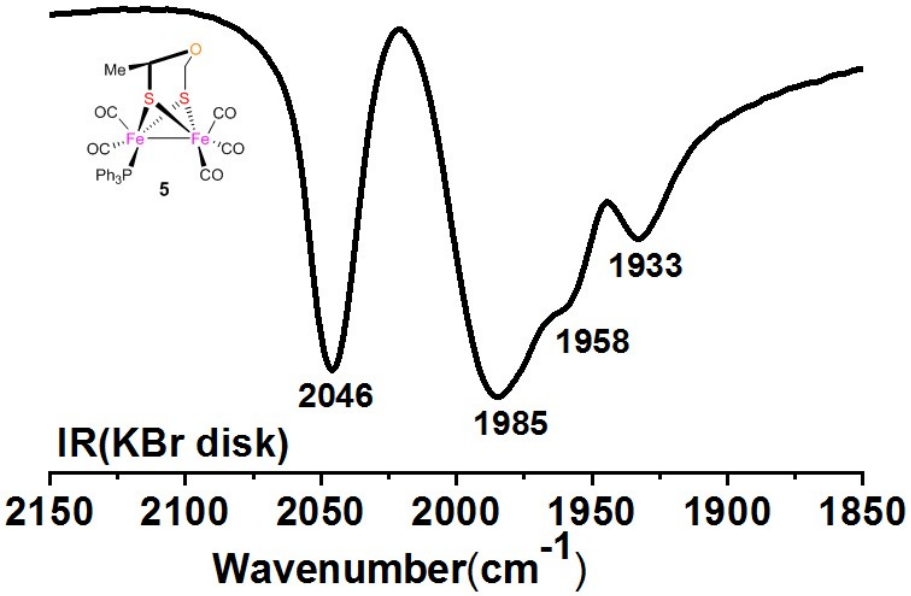

Figure S28. FT-IR spectrum of $Fe_2(\mu$-Meodt$)(CO)_5(PPh_3)$ (**5**) in KBr.

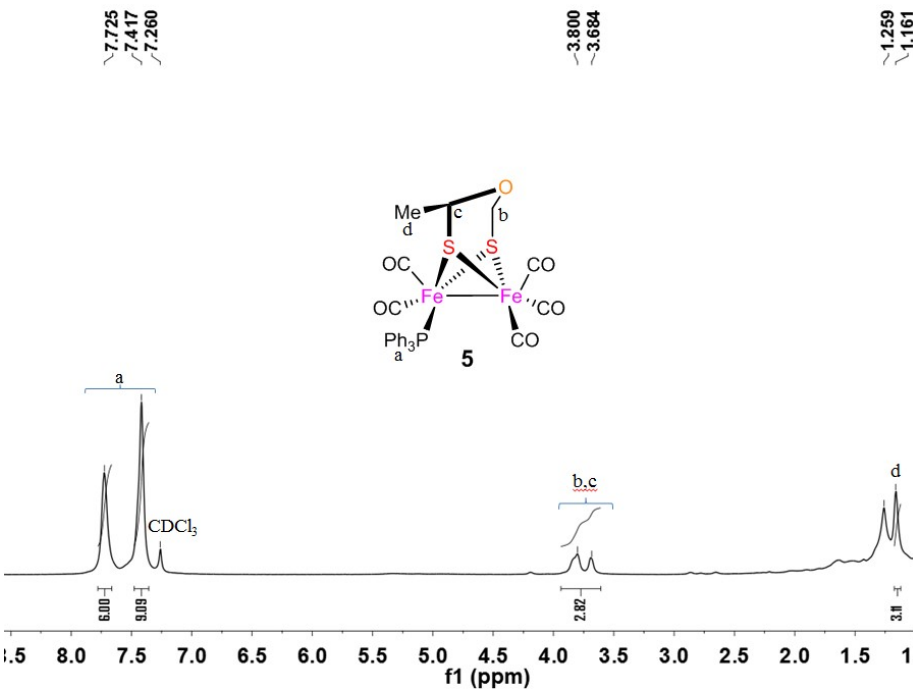

Figure S29. ^{1}H NMR spectrum of $Fe_2(\mu$-Meodt$)(CO)_5(PPh_3)$ (**5**) in $CDCl_3$ (600 MHz, TMS).

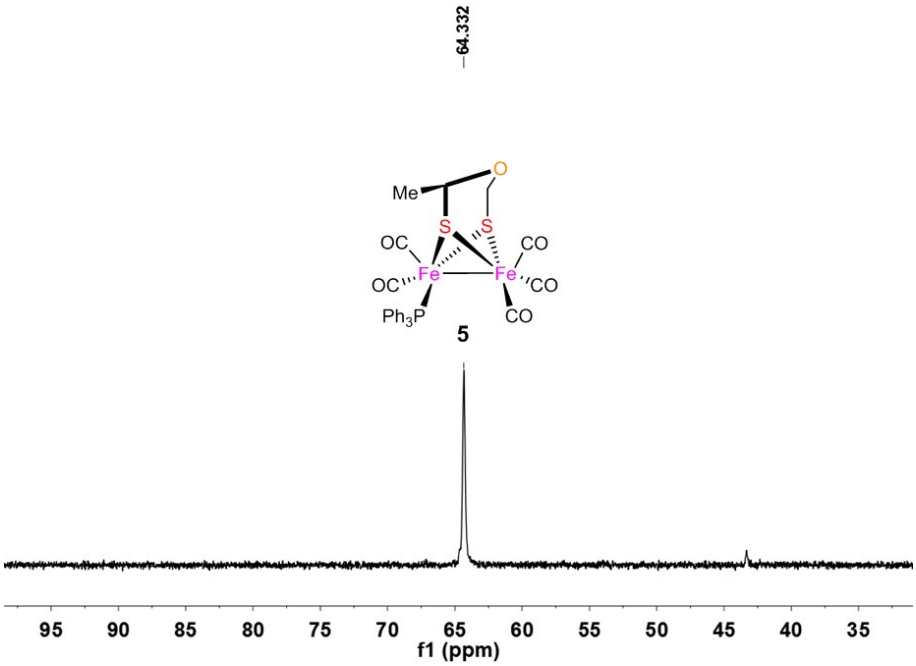

Figure S30. $^{31}P\{^{1}H\}$ NMR spectrum of $Fe_2(\mu\text{-Meodt})(CO)_5(PPh_3)$ (**5**) in $CDCl_3$ (243 MHz, 85% H_3PO_4).

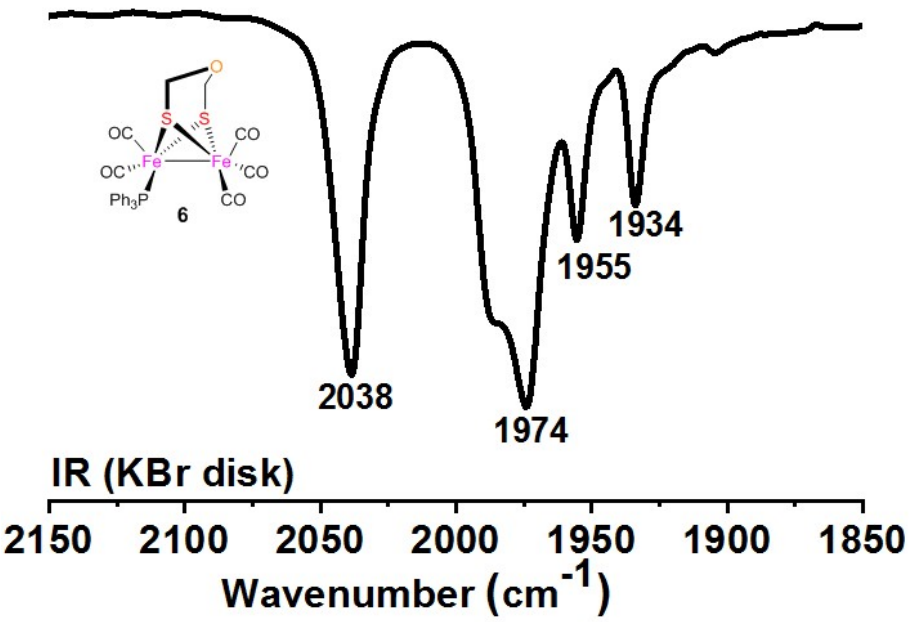

Figure S31. FT-IR spectrum of $Fe_2(\mu\text{-odt})(CO)_5(PPh_3)$ (**6**) in KBr.

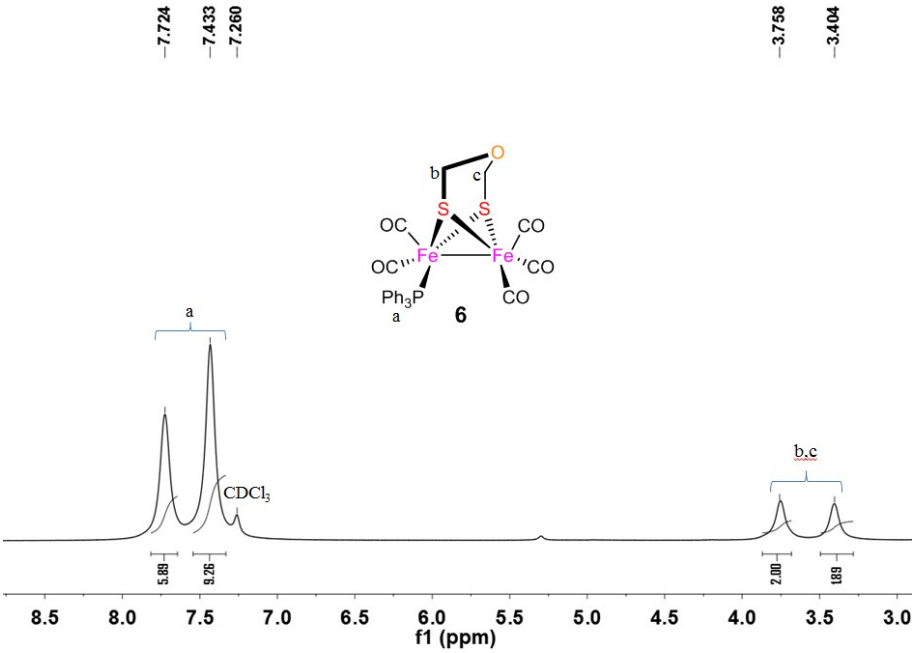

Figure S32. ^{1}H NMR spectrum of $Fe_2(\mu\text{-odt})(CO)_5(PPh_3)$ (**6**) in $CDCl_3$ (600 MHz, TMS).

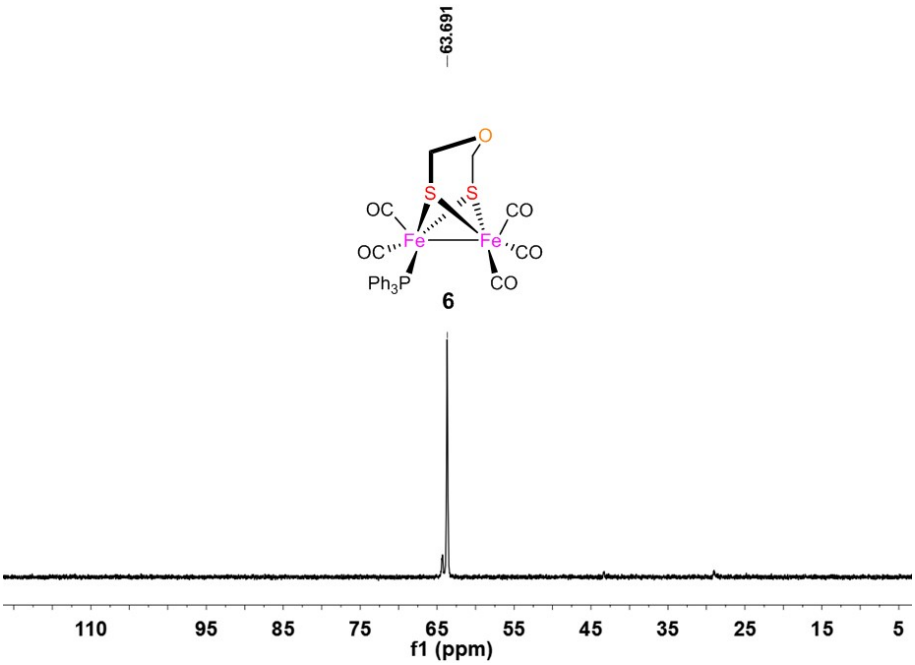

Figure S33. $^{31}P\{^{1}H\}$ NMR spectrum of $Fe_2(\mu\text{-odt})(CO)_5(PPh_3)$ (**6**) in $CDCl_3$ (243 MHz, 85% H_3PO_4).

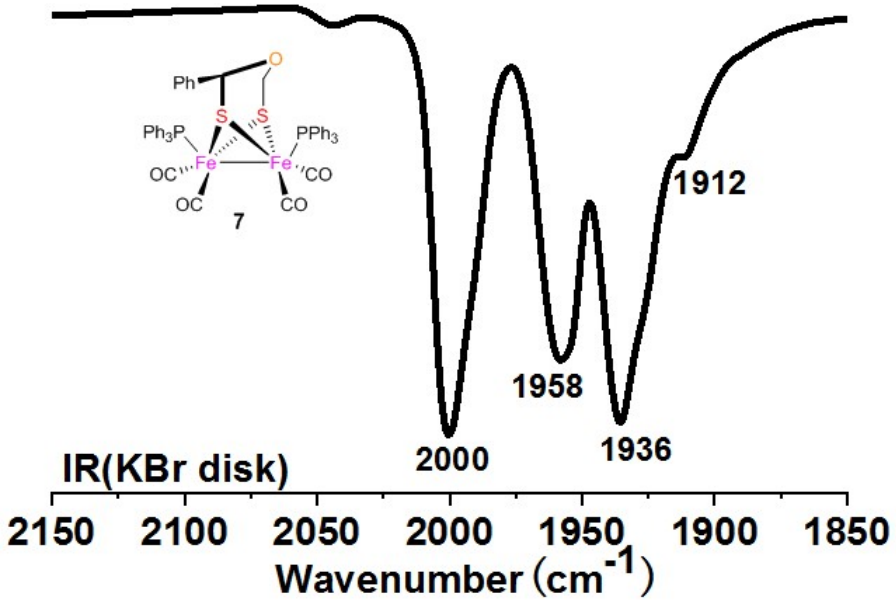

Figure S34. FT-IR spectrum of $Fe_2(\mu\text{-Phodt})(CO)_4(PPh_3)_2$ (**7**) in KBr.

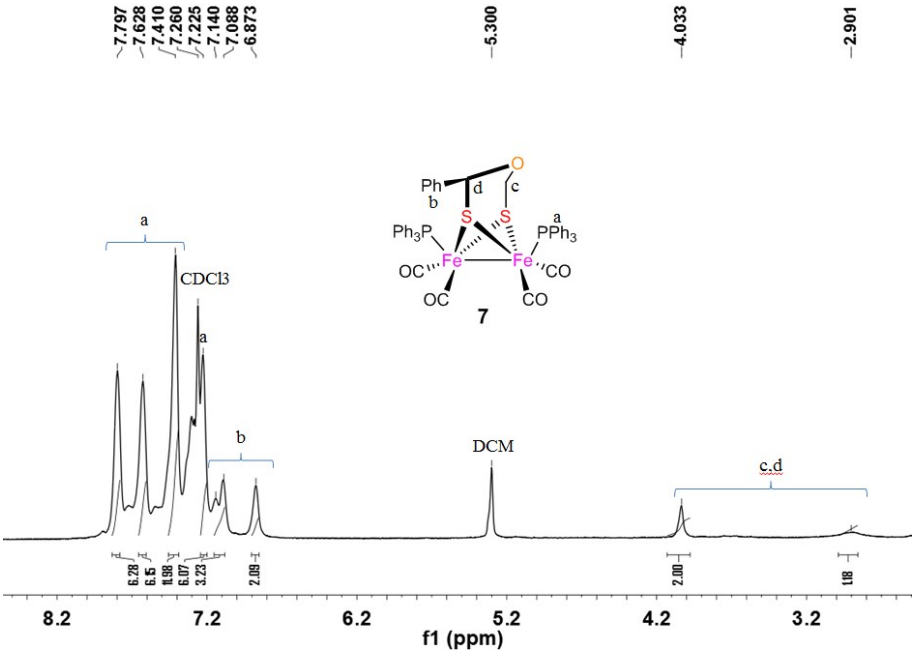

Figure S35. ^{1}H NMR spectrum of $Fe_2(\mu\text{-Phodt})(CO)_4(PPh_3)_2$ (**7**) in $CDCl_3$ (600 MHz, TMS)

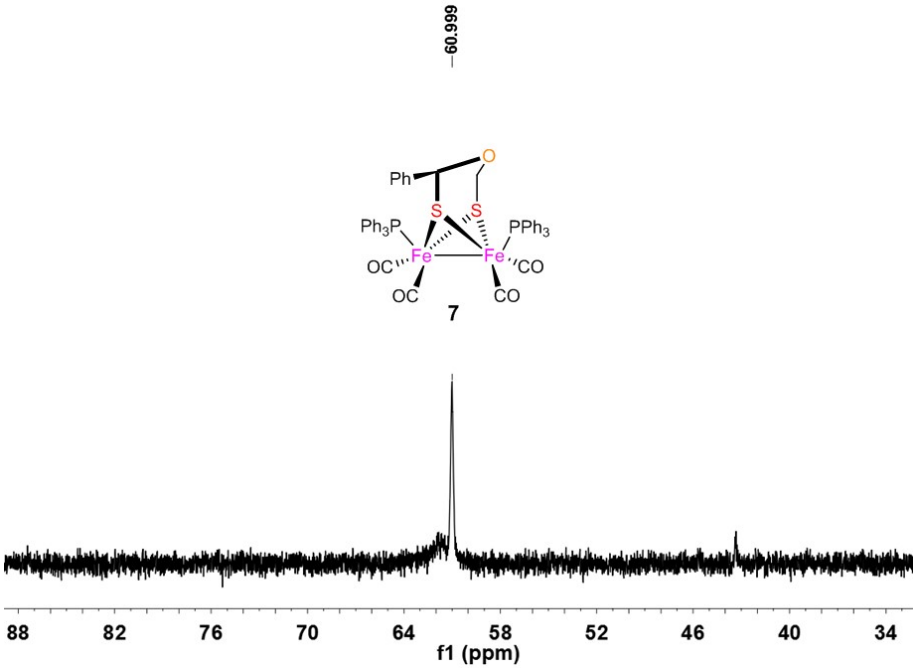

Figure S36. $^{31}P\{^{1}H\}$ NMR spectrum of $Fe_2(\mu\text{-Phodt})(CO)_4(PPh_3)_2$ (**7**) in $CDCl_3$ (243 MHz, 85% H_3PO_4).

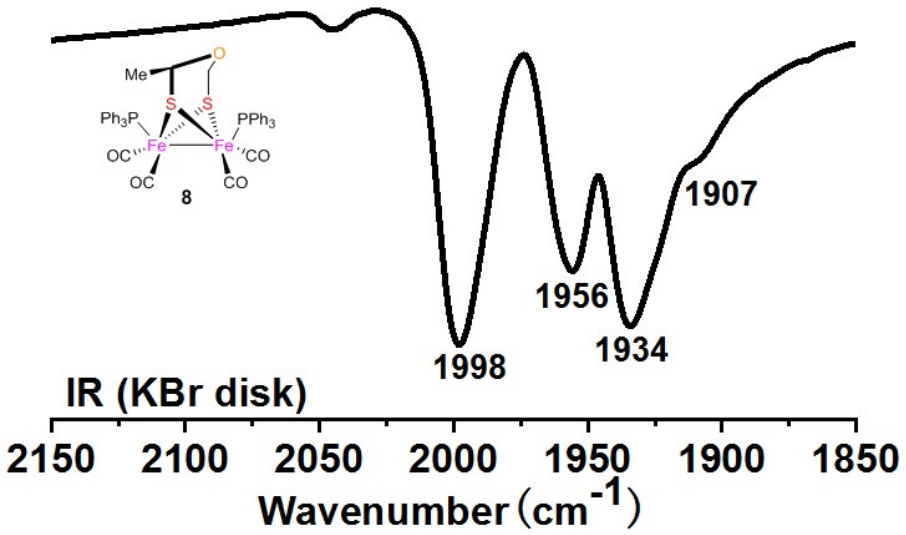

Figure S37. FT-IR spectrum of $Fe_2(\mu$-Meodt$)(CO)_4(PPh_3)_2$ (**8**) in KBr.

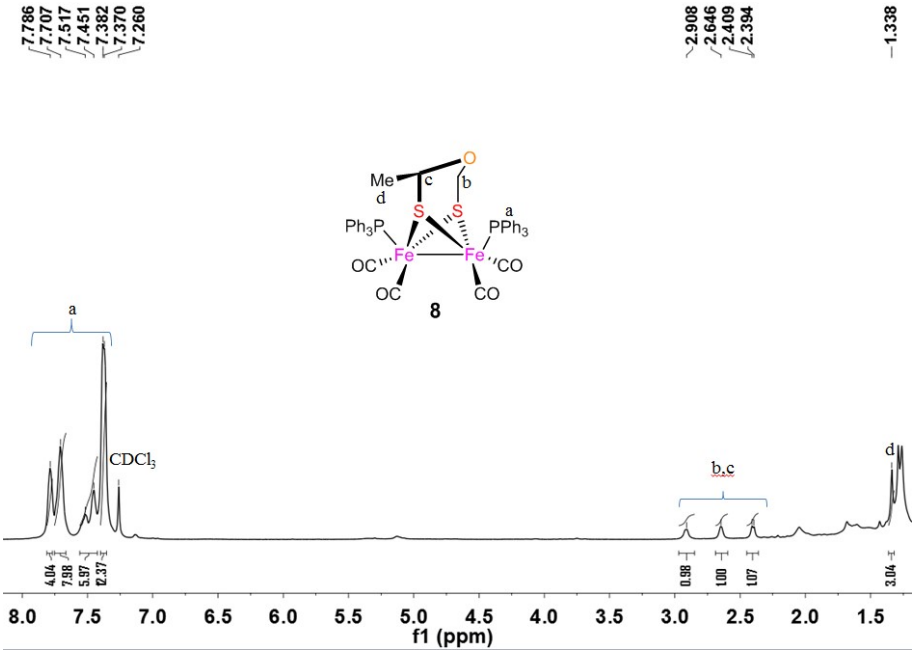

Figure S38. ^{1}H NMR spectrum of $Fe_2(\mu\text{-Meodt})(CO)_4(PPh_3)_2$ (**8**) in $CDCl_3$ (600 MHz, TMS).

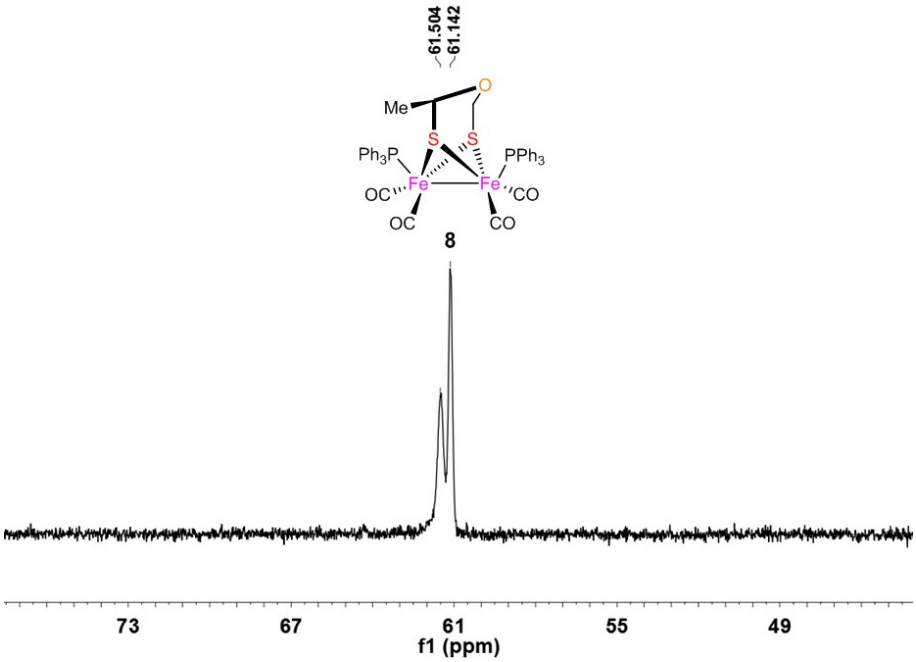

Figure S39. $^{31}P\{^{1}H\}$ NMR spectrum of $Fe_2(\mu\text{-Meodt})(CO)_4(PPh_3)_2$ (**8**) in $CDCl_3$ (243 MHz, 85% H_3PO_4).

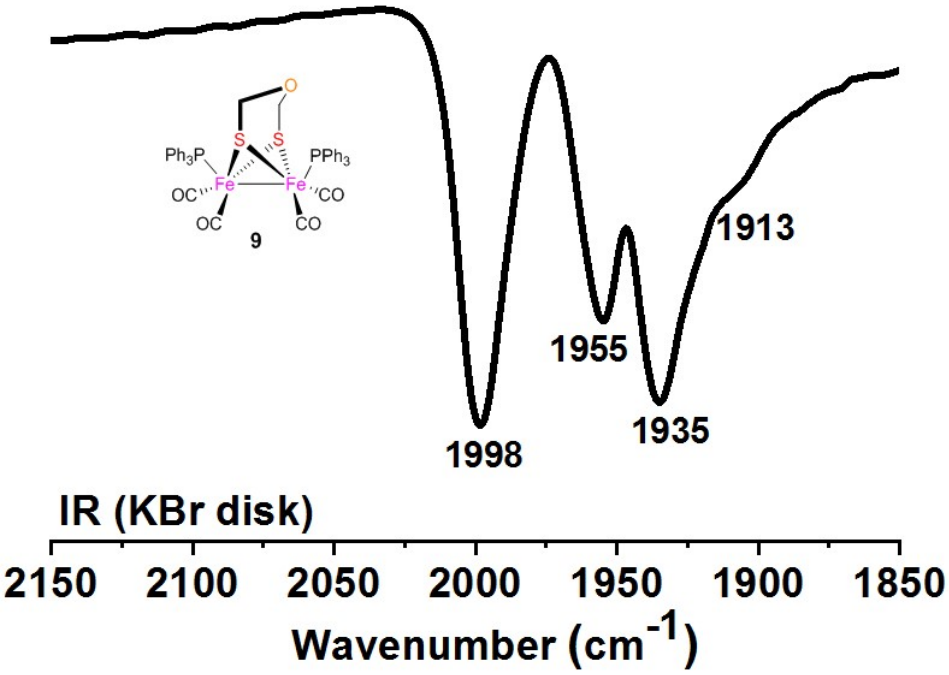

Figure S40. FT-IR spectrum of $Fe_2(\mu\text{-odt})(CO)_4(PPh_3)_2$ (**9**) in KBr.

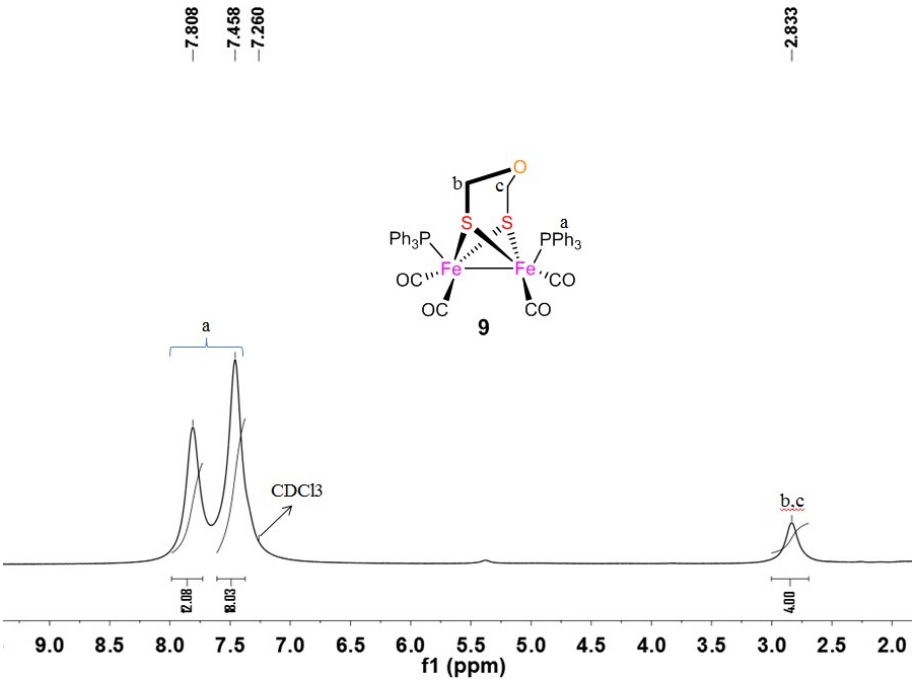

Figure S41. ^{1}H NMR spectrum of $Fe_2(\mu\text{-odt})(CO)_4(PPh_3)_2$ (**9**) in $CDCl_3$ (600 MHz, TMS).

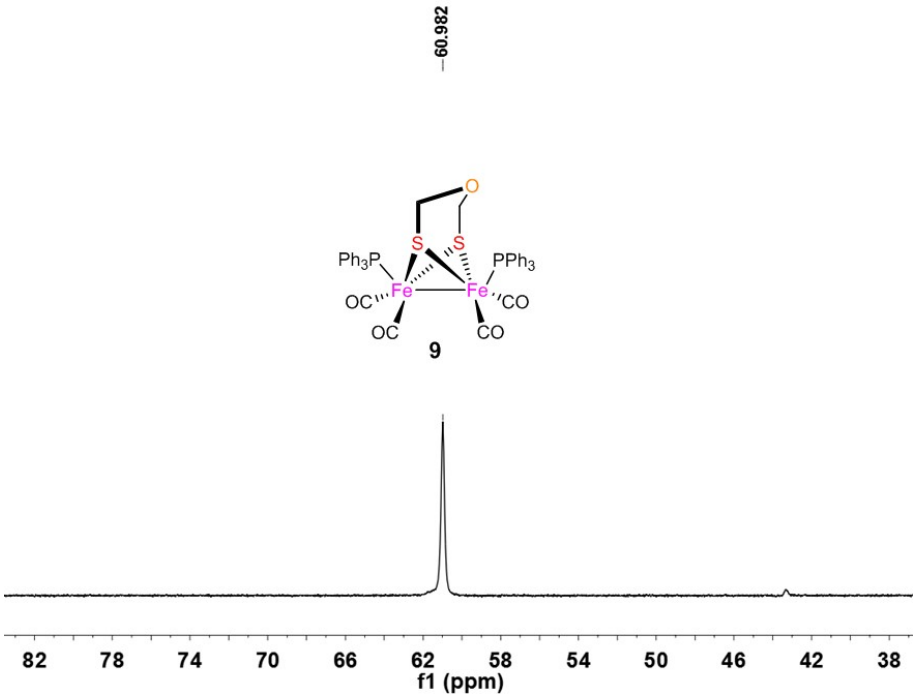

Figure S42. $^{31}P\{^{1}H\}$ NMR spectrum of $Fe_2(\mu\text{-odt})(CO)_4(PPh_3)_2$ (**9**) in $CDCl_3$ (243 MHz, 85% H_3PO_4).